Progress in Biomedical Engineering

ACCEPTED MANUSCRIPT

Review of in silico models of cerebral blood flow in health and pathology

To cite this article before publication: Stephen John Payne *et al* 2023 *Prog. Biomed. Eng.* in press https://doi.org/10.1088/2516-1091/accc62

Review of in silico models of cerebral blood flow in health and pathology

Authors

Stephen Payne[1], Institute of Applied Mechanics, National Taiwan University, Taiwan

Tamás István Józsa, Centre for Computational Engineering Sciences, School of Aerospace, Transport and Manufacturing, Cranfield University, College Road, Cranfield, MK43 0AL, United Kingdom; Department of Radiology and Nuclear Medicine, Amsterdam University Medical Center, location VUmc, Amsterdam Neuroscience, De Boelelaan 1117, 1118, 1081 HV Amsterdam, The Netherlands; Department of Engineering Science, University of Oxford, Parks Road, Oxford, OX1 3PJ, United Kingdom

Wahbi K. El-Bouri, Liverpool Centre for Cardiovascular Science, University of Liverpool & Liverpool Heart and Chest Hospital, Liverpool, UK; Department of Cardiovascular and Metabolic Medicine, Institute of Life Course and Medical Sciences, University of Liverpool, Liverpool, United Kingdom

[1] Corresponding author; stephenpayne@ntu.edu.tw

Abstract

In this review, we provide a summary of the state-of-the-art in the in silico modelling of cerebral blood flow and its application in in silico clinical trials. Cerebral blood flow plays a key role in the transport of nutrients, including oxygen and glucose, to brain cells, and the cerebral vasculature is a highly complex, multi-scale, dynamic system that acts to ensure that supply and demand of these nutrients are continuously balanced. It also plays a key role in the transport of other substances, such as rt-PA, to brain tissue. Any dysfunction in cerebral blood flow can rapidly lead to cell death and permanent damage to brain regions, leading to loss of bodily functions and death.

The complexity of the cerebral vasculature and the difficulty in obtaining accurate anatomical information combine to make mathematical models of cerebral blood flow key in understanding brain supply, diagnosis of cerebrovascular disease, quantification of the effects of thrombi, selection of the optimum intervention, and neurosurgical planning. Similar in silico models have now been widely applied in a variety of body organs (most notably in the heart), but models of cerebral blood flow are still far behind. The increased availability of experimental data in the last 15 years however has enabled these models to develop more rapidly and this progress is the focus of this review.

We thus present a brief review of the cerebral vasculature and the mathematical foundations that underpin cerebral blood flow in both the microvasculature and the macrovasculature. We also demonstrate how such models can be applied in the context of cerebral diseases and show how this work has recently been expanded to in silico trials for the first time. Most work

to date in this context has been performed for ischaemic stroke or cerebral aneurysms, but these in-silico models have many other applications in neurodegenerative diseases where mathematical models have a vital role to play in testing hypotheses and providing test beds for clinical interventions.

Table of Contents

1. Introduction

The human brain is a highly complex organ, but one that remains surprisingly poorly understood in many ways. It accounts for 25% of the body's glucose and 20% of the body's oxygen metabolism, supplied by 14% of total blood flow, Kety and Schmidt (1948). The cerebral vasculature is key in ensuring a continuous, sufficient supply of nutrients (essentially oxygen and glucose) to all brain cells. This means that cerebral blood flow (CBF) is very tightly controlled to match supply with demand at both a global scale and a local scale. Since oxygen diffuses slowly and is metabolised quickly, every brain cell lies within approximately 25 μm from a capillary vessel, Abbott et al. (2010). The cerebral vasculature is thus a highly complex, structurally heterogeneous, inter-connected network of blood vessels that provides a continuous supply of oxygen and glucose to brain tissue.

CBF changes in many physiological and pathophysiological conditions. It drops in a linear relationship with age during adulthood (with the rate of decline being dependent upon the location), in parallel with the decrease in metabolic rate with age, see for example the study by Ainslie et al. (2008). Due to stiffening of the vessel walls, there are significant changes in the pulsatile behaviour of CBF with age, with pulse wave velocity increasing substantially, see

for example the study by Vaitkevicius et al. (1993). Hypertension (prolonged elevated blood pressure), which is a significant risk factor in nearly all cerebrovascular diseases, has significant long-term effects on both the cerebral vasculature and CBF patterns. It has also been suggested that changes in the cerebral vasculature could provide early warning of neurological changes, such as Alzheimer's disease, Wardlaw et al. (2013).

Although changes in CBF are now known to be implicated in multiple neurodegenerative diseases, we will primarily focus on the role of CBF in stroke and the flow fields associated with aneurysms in this review, as this is the context in which most modelling of CBF (and the two major in silico trials to date) have been performed to date. Ischaemic stroke is caused by the blockage of a supply vessel to the brain with a clot, such that the tissue that is perfused via this vessel becomes starved of oxygen (unless alternatively supplied via a collateral vessel) and proceeds to cell death. Haemorrhagic stroke is caused by the rupture of a blood vessel, which leads to the pooling of blood in the extravascular space and a rise in intracranial pressure (ICP). Transient ischaemic attacks (TIA) are sometimes termed 'mini-strokes', but the relationship between these and 'full' strokes is not yet fully understood, with these not yet providing a reliable marker of future events, Wardlaw et al. (2015). An aneurysm is an abnormal ballooning in the wall of a blood vessel, caused by a localised weakness in the vessel wall; these most often occur at vessel bifurcations and can remain steady for decades, Ajiboye et al. (2015).

Clinical therapies for ischaemic stroke essentially aim at recanalization, either through breakdown of the clot using recombinant tissue-plasminogen activator (rt-PA), which acts to catalyse the conversion of plasminogen to plasmin and hence to break down the clot, or

through mechanical thrombectomy, which acts to aspirate the clot via a catheter inserted into the brain. Both therapies have proven clinical benefit in the 4-6 hours following stroke onset, Wardlaw et al. (2012), although both also have risks attached to them, which makes the outcome difficult to predict in individual subjects. For aneurysms, a wide range of devices has been developed to stabilise the ballooning, by covering the neck of the aneurysm with a stent and/or coiling within the aneurysm sac. As there are many factors involved, primarily due to the highly complex geometries, computational fluid dynamics (CFD) models of the flow in these local environments have been extensively used to guide treatment, Ishida et al. (2021).

This balance of risk and benefit in any clinical intervention has driven the need for computational models of CBF that can act as a test bed, both in the development of new interventions and in planning interventions for individual patients. A 3D model of the cerebral vasculature and CBF is clearly of significant clinical benefit in the context of the visualisation and quantification of stenoses, vessel occlusions and cerebrovascular malformations such as aneurysms as well as both ischaemic and haemorrhagic stroke, see for example Steinman et al. (2003), Meijs et al. (2017), Murayama et al. (2019), and Saxena et al. (2019).

Such computational models have been widely developed in other organs, for example the heart and the liver, so extending these to the brain is a natural step. However, the brain poses its own specific challenges in this context, and the work that has been performed is relatively preliminary in many areas. In this review, we thus aim to present a detailed overview of the approaches that have been taken to models of CBF, presenting the pathway to the development of in silico trials that can be used within a clinical context. We will thus provide

a guide to how CBF modelling is done, both in terms of theoretical and practical approaches. It is worth noting that the review focuses more on the arterial circulation rather than the venous circulation which reflects the balance of the literature.

We should explicitly mention here that we will exclude the cerebrospinal (CSF) circulation here for reasons of space, although there has been some work performed to model this, coupled to the cerebral vasculature, see for example Toro et al. (2022). The glymphatic system is particularly poorly understood and again this will be left to other reviews. Finally, although the coupling between CBF and oxygen transport is a very tight one with the cerebral vasculature ensuring a continuous sufficient supply of oxygen and glucose to brain cells, we do not have space to consider models of oxygen transport in the brain and the reader is referred to other sources, for example Payne 2017, for further detail in this context.

2. Cerebral vasculature in health and disease

2.0 Introduction

In this section, we briefly consider the anatomy and geometry of the cerebral vasculature, both in health and disease. We also consider the most common pathological conditions, in particular stroke and aneurysms, for which we will consider the most important clinical intervention models in more detail later.

2.1 Anatomy and geometry

The human cerebral vasculature is supplied by four blood vessels that pass through the neck into the brain: the left and right internal carotid arteries (ICAs) and the left and right vertebral

arteries (VAs). The VAs join to form the basilar artery (BA), which is then linked to the ICAs via the circle of Willis (CoW). The CoW is made up of the left and right anterior cerebral arteries (ACAs), the anterior communicating artery (AcA), the posterior cerebral arteries and the posterior communicating arteries (PcAs). The net result is that there are six major vessels that supply blood to the brain: the left and right middle cerebral arteries (MCAs), the ACAs, and the posterior cerebral arteries (PCAs). The cerebrum is thus often divided into six vascular territories for the purposes of modelling CBF. There are of course multiple smaller vessels that branch off from the large arteries, as the vasculature distributes itself through the brain into the different vascular territories, Figure 1.

It should also be noted that only around half the adult population has a complete circle of Willis, with this fraction being smaller in patient populations, see for example Papantchev et al. (2013) and Hindenes et al. (2020). There are many types of CoW variant, although the handful of most common variants comprise most cases, with age being a factor in the number of missing segments, Hindenes et al. (2020). This has important implications for collateral flow, which is a key marker of the response to ischaemia; this is normally graded on a scale of 0-4 based on angiography data, Higashida et al. (2003), and is known to be a factor in clinical outcome post stroke, Kleine et al. (2016).

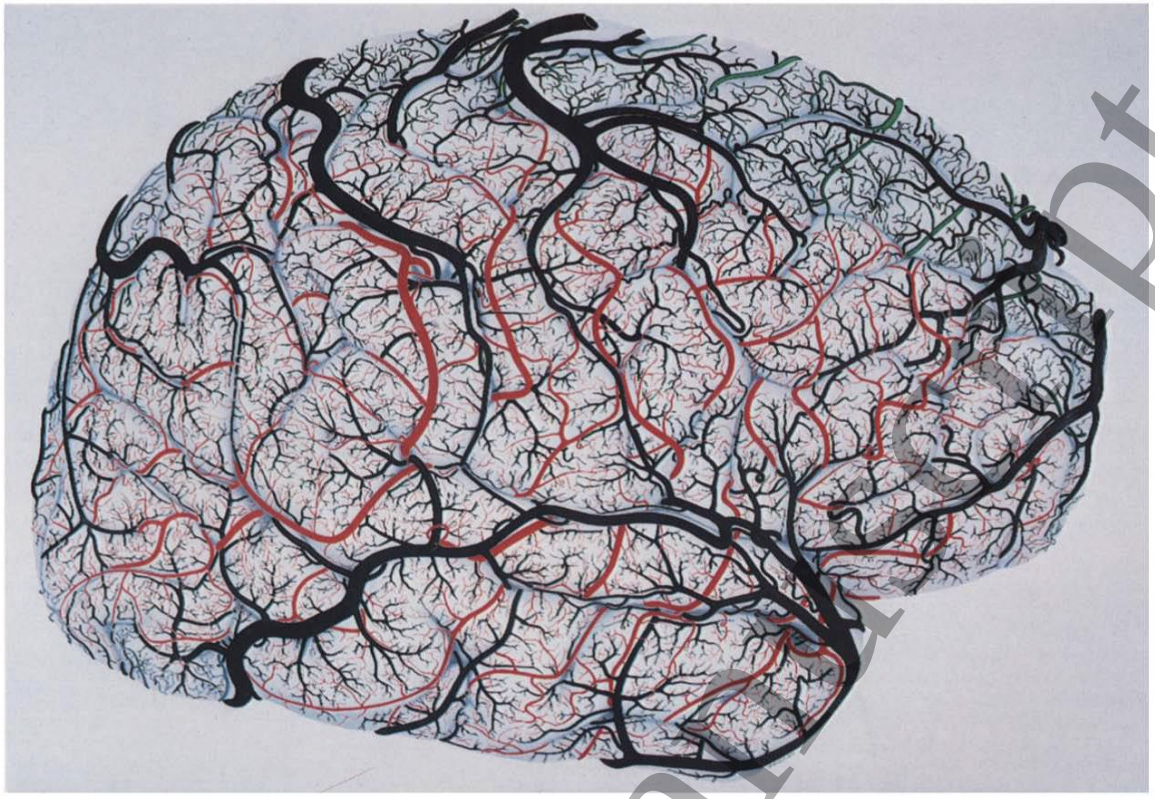

Figure 1 Cortical pial vessels. Red = tributaries of MCA; green = tributaries of ACA; blue = tributaries of PCA; black = veins. Reproduced with permission from Duvernoy et al. (1981)

The six supply routes form a network of large vessels that is commonly thought of as a bifurcating tree of ever-decreasing diameter and length. Arterial blood enters the individual territories via the leptomeningeal vessels (found on the cortical surface) and the penetrating / descending arterioles that 'dive' into the cortical tissue. These vessels are surrounded by a perivascular space, the Virchow-Robin space, that acts to clear interstitial fluids as part of the glymphatic system, Iliff et al. (2013) and Xie et al. (2013). In a similar manner to the large vessels, these continue to bifurcate, decreasing in diameter and changing in wall composition, until reaching the capillary bed, as shown in Figure 2. There is then a parallel venous

circulation, with postcapillary venules feeding into ascending venules and hence back into the (venous) pial circulation.

Different vessels feed and drain different layers, with some vessels penetrating the whole cortex before supplying the capillary bed, Duvernoy et al. (1981). The capillary vessel walls comprise both an endothelial layer, with endothelial cells coupled by tight junctions forming the blood-brain-barrier, and the basal membrane. The walls of arteries and veins also contain smooth muscle cells that play a key role in the regulation of tone and hence diameter; the role of pericytes, which surround the capillary vessels, in regulating flow has now become much clearer, see for example Hall et al. (2014).

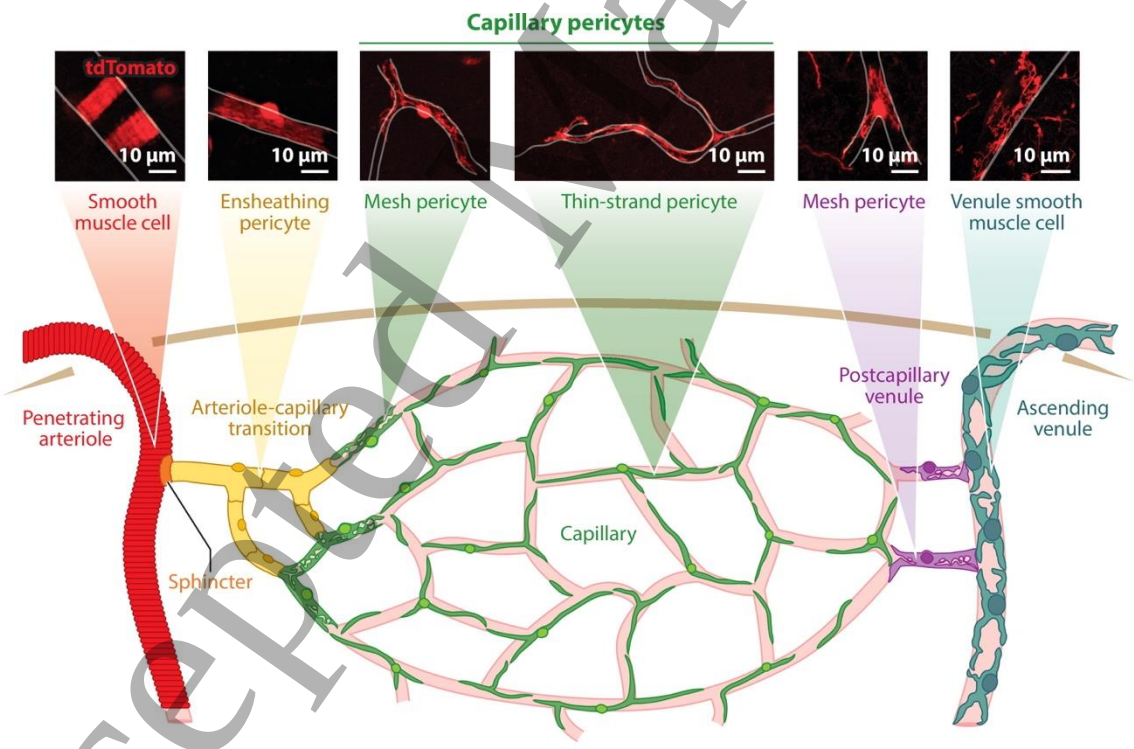

Figure 2 Schematic showing different microvascular generations in the cerebral circulation, reproduced with permission from Hartmann et al. (2022)

The capillary bed itself forms a highly interconnected network of vessels that ensure that no brain cell is more than approximately 25 μm from a capillary vessel, Abbott et al., (2010). The ascending venules (found in a 1:3 ratio to the penetrating arterioles in humans) then drain the blood back onto the cortical surface. These arteriole-capillary-venule structures can be considered to form units providing blood supply to specific territories, although the size of these units remains somewhat uncertain due to the often very small samples that available from animal models. This means that it is not yet clear what is a characteristic length for a representative elementary volume at this length scale[2].

There is a parallel venous circulation, where the sinuses drain towards the confluence of sinuses at the back of the head. At this point, fluid enters the transverse sinuses and moves towards the jugular vein via the sigmoid sinus. The jugular veins drain into the subclavian veins and then out of the head through the neck and into the heart via the superior vena cava. It should be noted that few computational studies have considered models of this component of the circulation. A schematic showing the different vasculature components and the corresponding length scales is shown in Figure 3. Quantification of the properties of the vascular tree is normally performed in terms of the Murray exponent. This generally drops from around 2 in larger vessels (such that reflections are avoided, Caro et al. (2012)) to close to 3 (for energy minimisation, Murray (1926)) in smaller vessels.

[2] SJP is grateful to Professor Andreas Linninger for a very informative discussion on this topic.

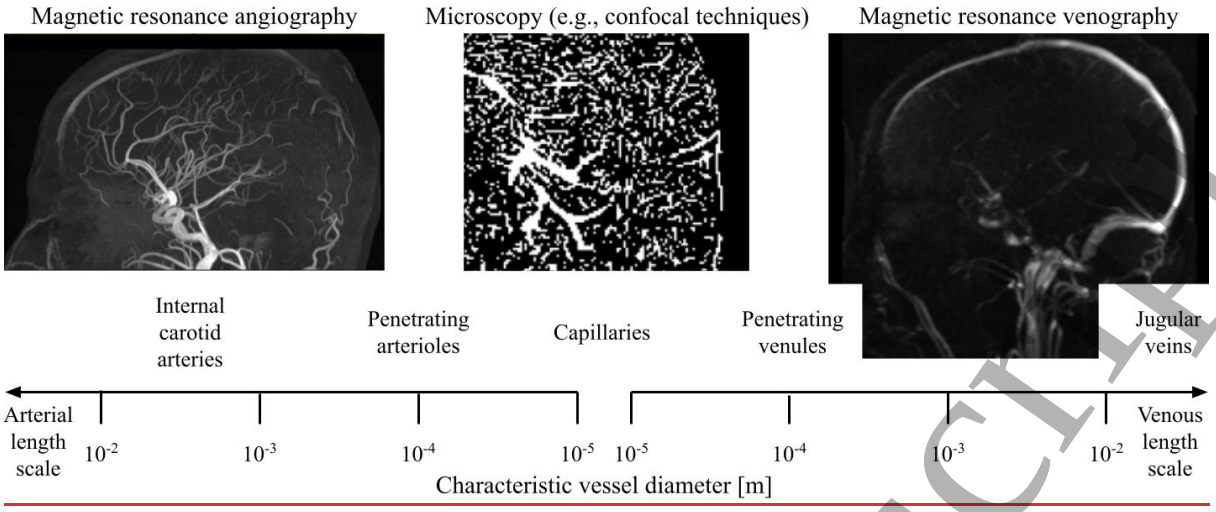

Figure 3 Relationship between imaging data and characteristic length scales. The microscopy image corresponds to rodent data publicly available thanks to Todorov et al. (2020)

The cerebral vasculature is of course a highly dynamic, active system that responds to multiple global and local stimuli to provide a tightly coupled relationship between local supply and demand. This control is now known to occur over a range of length scales, in both the arteriolar and capillary vascular beds. Many models of these multiple mechanisms have been proposed, but we will not consider this control further here as it is beyond the scope of this review. For further information, see Payne (2016). However, it should be considered carefully when developing models of the cerebral circulation as this is a key component of its behaviour and impaired regulation of CBF has been implicated in multiple diseases, including ischaemic stroke, Aries et al. (2010), dementia, den Abeelen et al. (2014), and traumatic brain injury, Czosnyka and Miller (2014).

2.2 Pathology and treatment

Ischaemic stroke is caused by the presence of a thrombus within a large vessel that blocks the flow through that vessel. Each thrombus is an individual mixture of fibrin, platelets, and other

blood components; for a review of clot properties and models, see Johnson et al. (2017). The composition of the thrombus is dependent on its origin, with large artery atherosclerosis, cardioembolism, and embolic stroke of unknown source being the three most common sources of stroke, Brinjikji et al. (2021). Two interventions have been shown to have clinical benefit in some patient groups, as described above: thrombolysis, see Wardlaw et al. (2012), and mechanical thrombectomy, see Berkhemer et al. (2015), Campbell et al. (2015) and Goyal et al. (2016). Essentially thrombolysis acts to dissolve the clot, and thrombectomy acts to remove the clot to restore flow, each with associated risks.

In the context of thrombolysis, it is known that the efficacy of the intervention depends on factors including the location, size, and composition of the clot, the flow field around the clot and the dose of the thrombolytic agent (varying doses have been adopted in different trials). Recombinant tPA is infused intravenously to dissolve the clot but can result in intracerebral haemorrhage (ICH) or be ineffective due to the clot location; computational models thus have a role in determining the optimal dose. In the case of thrombectomy, simulations aim to establish near-optimal stent retriever design which might also depend on thrombus composition and location. In addition, it is important to minimise embolisation which can subsequently cause micro-occlusions.

Intracranial aneurysms are characterised by an outpouching of the arterial wall due to localised thinning. Rupture can lead to poor outcomes, including cognitive disability and sudden death. Commonly found at bifurcations, aneurysms in the posterior circulation are less common and less likely to rupture than those found in the anterior circulation. Unruptured intracranial aneurysms under 7 mm in size tend to be asymptomatic and are often

incidentally detected in the course of neuroimaging for other reasons (hence the incidence rate has risen as brain imaging increases in popularity), Tawk et al. (2021).

Guidelines have been published for the management of unruptured intracranial aneurysms, Thompson et al. (2015). Intracranial aneurysms are now routinely treated via endovascular coiling or stenting rather than clipping, with clinical outcomes and protection against rebleeding and aneurysm rupture all shown to be good, Brisman et al. (2005) and Molyneux et al. (2005). The two most common complications are aneurysmal perforation and thromboembolism during endovascular coiling, which must be carefully managed and prevented, Ihn et al. (2018). Unruptured intracranial aneurysms are found in over 3% of the population, Weir et al. (2002), but between 50% and 80% of these do not rupture within the lifetime of the patient, Connolly and Solomon (1998). The balance of risks between treatment and non-intervention needs to be carefully judged.

It should be noted therefore that there remain relatively few cerebral interventions available, although these are now starting to be applied more widely in the population. The complications from intervention failure can, however, be catastrophic, which strongly support improved techniques to stratify patient groups more accurately and improved mathematical models to support decision making and intervention planning (the current state-of-the-art of which are described below).

2.3 Conclusion

In this section we have briefly explored the anatomy and geometry of the cerebral vasculature. We then considered the most common pathological conditions and their treatments, noting

that there are few available treatments yet, with mathematical models still to play their full part in the clinical intervention pathway.

3. Imaging the cerebral vasculature and blood flow

3.0 Introduction

In this section, we consider how quantitative information can be obtained about both the cerebral vasculature and cerebral blood flow on both a population level and for an individual subject. This will include both ex-vivo and in-vivo information and highlight the recent technical advances that enable far greater resolution to be obtained than even five years ago. We will, however, not give an overview of the techniques underlying these modalities, as there are many other excellent sources that provide a full description of these methods.

3.1 Reconstruction of the macrovasculature

Some of the earliest work into quantifying the anatomical and geometrical properties of the cerebral vasculature was performed by Duvernoy et al. (1981) in a pioneering study that injected low viscosity resin into 25 ex-vivo brains shortly after death. This enabled extremely detailed images to be obtained using Scanning Electron Microscopy (SEM), although limited quantitative data were published until the development of automated tools for vessel segmentation some 25 years later.

There are now several publicly available databases for the large vessels, some of which are listed in Table 1. The first such substantial database, noting earlier smaller datasets (number of subjects < 10) from Cool et al. (2003) and Dufour et al. (2011), was developed and published

by Wright et al. (2013), who examined a group of 61 young healthy subjects using 3 T three-dimensional time-of-flight magnetic resonance angiography (MRA); the database comprises digital reconstructions of the six major arterial trees from the internal carotid and basilar arteries down to the 'visible ending' of each branch, Figure 4. With this imaging resolution, this provided information down to a diameter of approximately 0.8-0.9 mm. Additional databases have now been made publicly available; although other studies have been performed, such as Viviani (2016), these are not publicly available at time of writing. Note that some studies are based on several data repositories from different centres. All these studies have been performed at 3 T, as this is clinically routine, although there have been some preliminary smaller studies at 7 T, see for example Nowinski et al. (2011) and the much-improved resolution available at higher field strengths should enable information down to smaller length scales to be obtained in future.

Study	**Number of subjects**	**Imaging modality**	**Data repository**
Wright et al. (2013)	61 young healthy subjects	3 T MRA	https://cng.gmu.edu/brava
Dunas et al. (2017)	167 elderly healthy subjects	3 T MRA	https://www.nitrc.org/projects/brainarteries
Bernier et al. (2018)	42 healthy subjects	3T MRA	https://github.com/braincharter/vasculature

Mouches and Forkert (2019)	544 healthy subjects	MRA	http://brain-development.org; http://insight-journal.org/midas/community/view/21

Table 1 Details of publicly available data sets for the cerebral macrovasculature

These datasets now provide researchers with a very substantial amount of information in large numbers of subjects (noting that all these remain confined to healthy subjects); more recent studies also provide probability artery-specific atlases from which any arbitrary number of virtual cerebral macrovasculatures can be constructed in future. Fewer studies have mapped the venous circulation; hence this is less common and remains more poorly quantified.

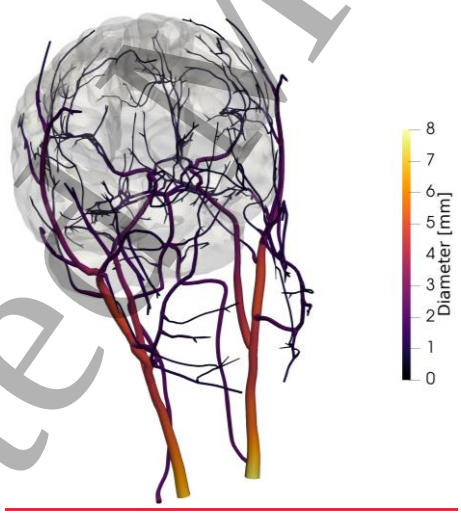

Figure 4 Reconstruction of cerebral arteries based on angiography data (an example of which is shown in Figure 3)

The acquisition and quantification of these data both rely heavily on accurate segmentation of these vascular images, which remains a key challenge due to the complexity of the available

data. Early methods relied on manual input, which rendered the segmentation of large volumes impracticable, due to the complex multi-scale nature of the segmentation, see for example the early reviews by Luo and Zhong (2005) and Lesage et al. (2009). Additionally, differing imaging protocols and modalities, inconsistent contrast, intensity inhomogeneities, shadow effects and the small size of the smaller vessels have all served to make robust segmentation methods highly challenging to develop successfully, Yu et al. (2016), Ajam et al. (2017), Zhao et al. (2018), Deshpande et al. (2021).

Multiple methodologies have thus been proposed to tackle this problem, see for example Flasque et al. (2001), Passat et al. (2006), Gao et al. (2012), Wang et al. (2015), Hsu et al. (2017), Meijs et al. (2017), Chen et al. (2018), Zhao et al. (2018), Livne et al. (2019) and Goswami et al. (2020), with a recent summary of these cerebral vascular segmentation methods and their advantages and disadvantages provided by Deshpande et al. (2021). In this study, they propose and apply successfully automated vessel-enhanced filters that can be applied across both MRA and invasive computed tomography angiography (CTA) images for the first time. The process is shown in Figure 5, although the authors note that the methodology remains limited by the quality and resolution of the original images. It should also be noted that in the context of vascular reconstruction the distinction between manual and automated methods is perhaps somewhat blurred, with the need in many algorithms to label 'seed points' to initialise the algorithm.

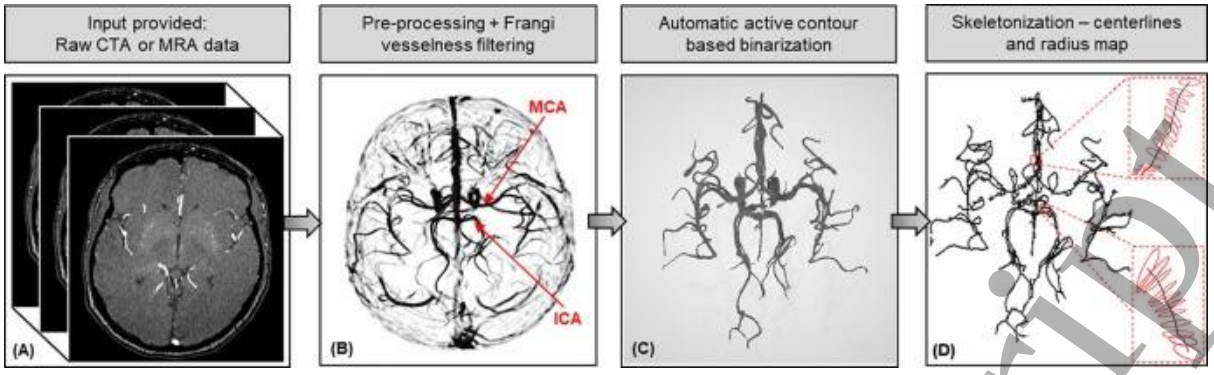

Figure 5 Vessel segmentation and skeletonization methodology, proposed by and reproduced with permission from Deshpande et al. (2021)

Such datasets can generally only reach a resolution of around 1 mm (due to the field strength), thus proving unable to provide measurements down to the length scale of the pial circulation. Higher field strength imaging has improved the resolution that can be achieved in vivo, but ultra-high-resolution angiography will be required to characterise the pial circulation in vivo, Bollmann et al. (2022), and this remains one of the biggest challenges in modelling CBF. A recent review of the evolution of human brain atlases, Nowinski (2021), has highlighted the enormous increase in imaging data and the gradual translation to clinical application, together with the need for a standard framework to be developed and widely adopted for these datasets.

The ability to examine these large datasets means that, in a similar manner to the detailed characterisation of the microvasculature, described below, the properties of the macrovasculature can be characterised to quantify length and radius distributions and aspect ratio and tortuosity in these networks, see for example the analysis by Mut et al. (2014). In addition, more detailed topological approaches have been adopted to quantify the properties of the arterial trees, see for example Bendich et al. (2016).

Changes to these macrovascular properties can be an indication of both altered function and increased risk of pathophysiology, Gutierrez et al. (2015), including atherosclerosis, Kim et al. (2015), and stroke, Lemasson et al. (2016). Vascular remodelling (e.g., the wall mechanical properties) can occur after ischaemic stroke, Liu et al. (2014), and this is an important aspect of the longer-term treatment of these patients although one that has yet to be included in any mathematical model of CBF. Changes in the cerebral macrovasculature properties are thought to be implicated in the progression of several neurological diseases, including Alzheimer's disease, Arvanitakis et al. (2016).

Healthy ageing has also been shown to have a significant effect on the macrovasculature, including the CoW structure, Hedman et al. (2012), and is a major risk factor for cardiovascular diseases, with mortality rates from cardiovascular disease increasing exponentially with age in later life, Ungvari et al. (2010). Studies have shown vessel wall thickening, Farkas et al. (2006), increased stiffness, Xu et al. (2017), increased tortuosity, Kamenskiy et al. (2015), and dilation, Gutierrez et al. (2016), reduced number of branches and average order, Chen et al. (2018). Interestingly, however, cerebral autoregulation has been shown to be unaffected by ageing, Carey et al. (2000) and van Beek et al. (2008), indicating that even though there are very large changes to the cerebral vasculature, the active response to changes in blood pressure is maintained with age, Payne (2016).

3.2 Reconstruction of the microvasculature

The surface layer of brain tissue is termed the cerebral cortex; this 2-4 mm thick layer plays a key role in many brain processes, including memory, perception, and language. The folded

arrangement increases the surface area many times, and it is divided into four lobes (temporal, occipital, parietal, and frontal). The surface layer comprises grey matter, with the deeper matter being made up of white matter; these are named after the shading found in imaging data and reflect the different compositions (grey matter has many neuronal cell bodies, but few axons, whereas white matter has many axons but few neuronal cell bodies).

The large cerebral arteries, detailed in the previous section, follow the cortical surface, then feed into a complex network of pial arteries (with a similar pial venous circulation to drain the cortex). These pial arteries bifurcate into penetrating arterioles that drive blood into the cortex and the mesh-like structure of the capillary bed. Since this is beyond the imaging limit discussed above, information about the microcirculation is limited and has only been obtained from either ex vivo brains or *in vivo* imaging of animal brains. Recently, *in vivo* imaging of human cerebral microcirculation has become possible in extreme cases (when open-skull surgery is required) using optical polarization spectral imaging, although little data have yet been made available, Pennings et al. (2004).

The first study to quantify the statistical properties of the human cerebral microcirculation was that of Cassot et al. (2006), which was based on a re-examination of the ex vivo data presented by Duvernoy et al. (1981) for the collateral sulcus in the temporal lobe (based on the quality of the injection) using confocal laser scanning microscopy (CLSM). A similar study was performed in the macaque around the same time, Weber et al. (2008). In these studies, cortical blood vessels were shown to be centred around pial draining veins, each of which is supplied by between three and six penetrating arterioles. The relationship between the diameter of a pial draining vein and the volume of the surrounding neuronally activated area

also provides a clear link between the vascular response to activation and the functional blood oxygen level dependent magnetic resonance imaging (fMRI-BOLD) signal, Lorthois et al. (2011). Models of the BOLD-fMRI response have thus been constructed from such detailed imaging data from first principles, Gagnon et al. (2015).

The need for accurate vessel diameter measurements (due to the inverse fourth power relationship with cerebrovascular resistance) means that submicron spatial resolution is required to capture reliably the smallest capillaries (diameter of about 8 microns). Whilst human (and primate) high-resolution imaging data of the microcirculation is severely limited, there are far more data available from rodent imaging. Techniques that have been used include two-photon microscopy with laser ablation to image fluorescently labelled microvasculature, Tsai et al. (2003) and Tsai et al. (2009); synchrotron radiation-based X-ray microscopy to obtain tomographic microvascular images, Reichold et al. (2009) and Guibert et al. (2010); micro-optical sectioning tomography, Xue et al. (2014); selective plane illumination microscopy, Erturk et al. (2012); optical coherence tomography, Marchand et al. (2020); and three photon microscopy, Horton et al. (2013).

One example of CLSM imaging and subsequent segmentation is shown in Figure 6. It should be noted that when modelling the human cerebral microcirculation, rodent data are often relied upon and, for the capillary bed at least, are representative of the human cerebral microcirculation up to a scaling, Smith et al. (2019). For reasons of space, we refer the reader to the review by Schmid et al. (2019) about the detailed properties of the cerebral microvasculature, including its density, topology, and regulation.

Generating blood flow simulations from the imaged data requires segmentation and reconstruction of these networks. Unlike when segmenting the macrocirculation that has far fewer vessels and often good signal-to-noise ratio (see previous section), segmenting the microcirculation requires tackling dense networks with complex connectivity, often poor signal-to-noise ratios, and movement and slicing artefacts, as well as limited depth-penetration. As a result, a lot of manual post-processing has often been required (see Cassot et al. 2006) which has inevitably resulted in a dearth of segmented data, Gagnon et al. (2016). Improved segmentation processes that utilise deep learning have recently been developed, although these are still semi-automated and require ground truth annotations to prove validity, Tahir et al. (2021). Many of these segmentation models have been developed for ophthalmic images, Leahy et al. (2015), Sharma et al. (2022) and Zhao et al. (2015).

Once a network has been accurately reconstructed, its statistical properties can be calculated. These normally include statistical distributions for vessel diameter and length, volume and surface densities, tortuosity, and orientation, as well as diameter ratios and branching angles. These distributions allow for the generation of statistically accurate microcirculation networks, avoiding the need to segment further images. The properties extracted from the images depend upon the specific brain region, although there is not yet any comprehensive study of how these vary across the brain. The original study by Cassot examined two blocks of the same region and showed that the statistical properties are very similar indicating that they are likely to be similar over short length scales, but these may vary over larger length scales, Shaw et al. (2021). A recent review found no differences in drops in blood flow with age and Alzheimer's disease between brain regions, Graff et al. (2022).

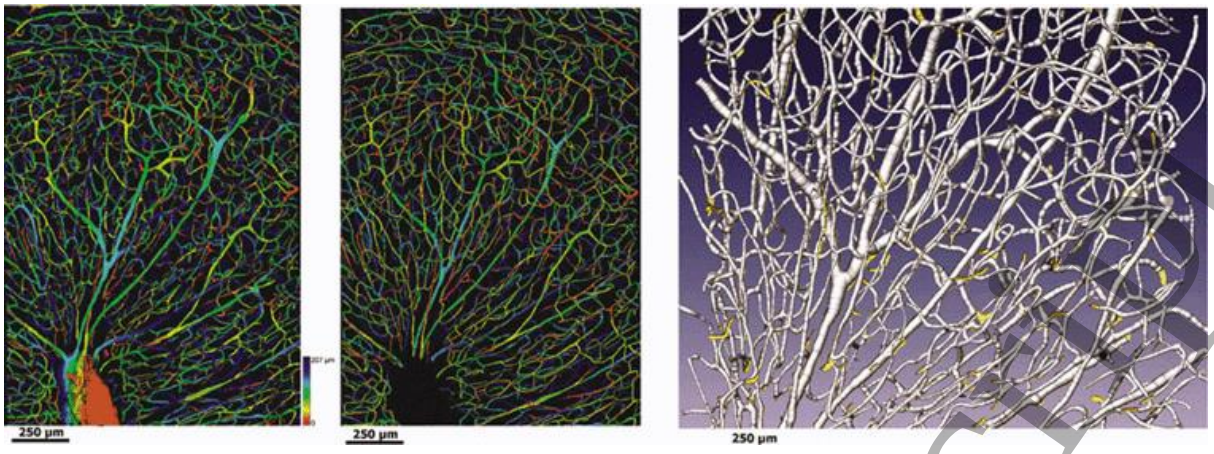

Figure 6 Example of confocal laser scanning microscopy imaging of the human cerebral microcirculation and subsequent reconstruction. Reproduced with permission from Cassot et al. (2006).

Several classification systems have been developed to label vessels dependent upon their connection to the remainder of the network. Calculations have shown that the networks predominantly comprise bifurcations (around 95% of nodes) with the remainder largely being trifurcations. The Strahler system and the Kassab system have both been used in this context; these essentially build up generation levels from the terminal branches using rules that depend upon the connections and the vessel diameters. This then enables vessel properties to be calculated based upon generation number and often Horton's law is used to postulate a power law relationship. Scaling laws have been extensively used in the coronary circulation, Huo and Kassab (2012), and these could be applied more widely to the cerebral circulation in future. Parameterisation of the network properties then allows for the reconstruction of statistical models that are representative of the underlying network.

Numerous methods exist for the reconstruction of these microcirculatory models. Voronoi tessellation has often been used to generate the capillary bed, Safaeian and David (2013),

Smith et al. (2019), with constrained constructive optimisation (CCO) used for the tree-like branching arterioles or venules, Linninger (2013). Matching statistical properties such as radii, length ratios, and densities through minimum spanning trees has been used to generate statistically accurate networks, Su et al. (2011), El-Bouri and Payne (2016). Angiogenesis based methods have also used to generate tree like structures, Schneider et al. (2012), as well as double bifurcation closures for capillary beds, Hartung et al. (2021). A partial list of reconstructed networks can be found in Table 2 highlighting the many different approaches that have been proposed.

The key parameter that 'encodes' information about the microcirculation is the permeability tensor. This can be calculated both from reconstructed networks and real networks and provides a concise metric for comparison of the microcirculation behaviour. It thus also enables quantitative comparisons to be made between different conditions: for example, the study by Gkontra et al. (2019), which, although in the porcine coronary microcirculation, showed that the measured permeability tensor dynamically changes in the seven days following myocardial infarction. Computational modelling in the cerebral circulation has also shown that the permeability changes in response to microthrombi (with the changes dependent upon the type of clot and the choice of thrombectomy procedure), El-Bouri et al. (2021), and these changes have been recently validated in animal models, Xue et al. (2021) and Xue et al. (2022). Gaining a quantitative understanding of changes in the permeability tensor is a concise way of providing a better understanding of the response both to ischaemia and to therapies such as mechanical thrombectomy.

Author	Species	Cap.	Pen. Vessels	Type of Model	Number of Vessels	Model Size - Length x Width x Depth (μm)^3
Zagzoule & Marc-Vergnes (1986)	Human	Y	Y	Lumped Parameter, 2D	316,858	Whole brain
Secomb et al. (2000)	Rat	Y	N	Cast, 3D	50	140x150x160
Beard (2001)	Rat	Y	N	Cast, 3D	50	150x160x140
Boas et al. (2008)	Rat	Y	Y	Vascular Anatomical Model, 2D	254	N/A
Fang et al. (2008)	Rat	Y	Y	Cast, 3D	N/A	230x230x450
Reichold et al. (2009)	Rat	Y	Y	Cast, 3D	N/A	N/A (volume 2.8 mm^3)
Guibert et al. (2010)	Marmoset	Y	Y	Cast, 3D	16,000	N/A (volume 18 mm^3)
Lorthois et al. (2011)	Human	Y	Y	Cast, 3D	10,318	N/A (volume 1.6 mm^3)

Su et al. (2011)	Human	Y	N	Statistical, 3D	1073	500x500x500
Safaeian and David (2013)	Human	Y	N	Statistical, 3D	492	600x380x250
Blinder et al. (2013)	Mouse	Y	Y	Cast, 3D	25,498 (average)	1200x1450x1900
Linninger et al. (2013)	Human	Y	Y	Both, 3D	256,000	3000x3000x3000
Gagnon et al. (2015)	Mouse	Y	Y	Cast, 3D	N/A	600x600x662
El-Bouri and Payne (2015)	Human	Y	N	Statistical, 3D	~2,000	625x625x625
El-Bouri and Payne (2016)	Human	N	Y	Statistical, 3D	1000+	1000x1000x2500
Schmid et al. (2017)	Mouse	Y	Y	Cast, 3D	23,496 (average)	1130x1130x1480 (average)
Gould et al. (2017)	Mouse	Y	Y	Cast, 3D	23,496 (average)	1130x1130x1480 (average)
Hartung et al. (2021)	Mouse	Y	Y	Statistical, 3D	Whole brain	Whole brain

Table 2 List of models of the cerebral microvasculature found in the literature. The 'Type of Model' refers to the architecture/geometry of the model.

Given that studies are often performed in networks obtained from animal models, it should be noted that there are multiple, significant, differences between the anatomical and geometrical properties of rodent and human microcirculations, which have been described in detail by Schmid et al. (2019). Although comparisons can be made between animal models and computational models of the human microcirculation, care must be taken to ensure that the comparisons are reasonable with suitable scaling factors normally being required.

As for the macrovasculature, ageing is known to affect the properties of the cerebral microvasculature. Reduced microvascular density, Brown and Thore (2011), and plasticity, Riddle et al. (2003), have both been shown in the cerebral microvasculature. Animal models have also shown reduced haematocrit, reduced capillary density and higher capillary transit time heterogeneity in the transition from middle age to old age, Moeini et al. (2018) where conversion between mouse age and human age can be performed using a sliding scale, Flurkey et al. (2007), Dutta and Sengupta (2016) and Agoston (2017), enabling the parameters to be translated from animal to human, as done in Graff et al. (2021).

These studies indicate that the microvasculature robustness to changes in arterial oxygenation reduces in old age. Although many properties of the cerebral microcirculation appear to change linearly with age, the overall change in behaviour is strongly non-linear and a 'tipping-point' past which any further changes have very significant effects on perfusion has been proposed. Such effects have also been shown in other studies, Xue et al. (2021), where the strong non-linearity of the response has again been identified.

3.3 Measurements of cerebral blood flow

There are very many imaging modalities that can be used to provide information about CBF (and cerebral blood volume, CBV). As this is an enormous topic, we will only very briefly mention the most common modalities here in the context of obtaining information that can be applied directly in developing a model of CBF in humans. For a more detailed coverage of this subject in this context, the reader is referred to Payne (2017).

It should first be noted that there is a difference between velocity, volumetric flow rate (flow) and perfusion, which is important to consider in the context of modelling. Velocity is a vector, usually measured in cm/s. From the velocity field, the volumetric flow rate is defined based on surface integration leading to a scalar, usually measured in ml/min, to represent the amount of blood delivered by the vessel (or vessels) per unit time. Finally, perfusion is a scalar, usually measured in ml/100g/min, accounting for volume flow rate to a given brain tissue mass contained within in a specific volume (e.g., voxel). We note that a perfusion vector might be introduced although this is rarely considered, and most usually perfusion is taken to be the net flux from the arterial compartment to the capillary compartment (noting that this does depend upon precisely where the boundary is placed between the two compartments, see Figure 2). Perfusion is typically around 50-60 ml/100g/min in grey matter (and a factor of around 2.5 lower in white matter), or around 0.009-0.1 s^{-1} in SI units (assuming that tissue density is that of water).

Flow is often measured using transcranial Doppler (TCD) ultrasound (normally in 2D, although more recently this has been extended to 3D, Correia et al. (2016)). This is based on

measurement of the Doppler shift and was first performed in humans by Aaslid et al. (1982); this Doppler shift can be converted to velocity, although knowledge of the vessel cross-sectional area is needed to convert this to flow. TCD is very simple and inexpensive to use, making it a popular choice for many studies, although there is no spatial resolution beyond left side and right side, and it cannot be used in all subjects. TCD measurements have also been used in conjunction with simple compartmental models to estimate parameters such as arterial compliance, Kim et al. (2009), potentially providing low-cost methodologies for estimation of key cerebral haemodynamic parameters, Uryga et al. (2019).

Optical techniques that have been commonly used in humans include near infra-red spectroscopy (NIRS), Jobsis (1977), and diffuse correlation spectroscopy (DCS), Boas et al. (1995). The former is based on optical absorption to measure changes in haemoglobin concentration whereas the latter is based on changes in scattering caused by the movement of red blood cells. These methods can provide excellent time and spatial resolution (although only to a certain depth) but are limited by being less direct measurements of CBF, containing both an intracerebral and an extracerebral component, which must be separated out, normally using a mathematical model of the cerebral circulation, Moroz et al. (2012).

Perfusion is measured using one of several available imaging modalities, primarily computed tomography (CT), positron emission tomography (PET), single-photon emission computed tomography (SPECT), or magnetic resonance imaging (MRI). Each of these modalities can also be used to measure other parameters such as cerebral blood volume. All have their individual advantages and disadvantages in this context, in terms of spatial resolution, signal-to-noise ratio, and contrast-to-noise ratio, Smith and Webb (2011). CT and MRI are the most

commonly used modalities, both in clinical studies and in research studies. Note that all these modalities require the use of a kinetic model to map the movement of a tracer (either endogenous or exogenous) through the cerebral vasculature. These models are typically highly simplified compartmental models based on the use of Fick's principle, and reviews of these models in this context can again be found in Payne (2017).

It should finally be noted that reproducibility between different modalities remains a major challenge in this area, meaning that care needs to be taken in comparing results obtained using different modalities, or even the same modality in a different machine. One application of the models described in this review is to simulate the movement of tracers and hence to provide estimates of the accuracy of these compartmental models through more detailed validation at smaller length scales. There also exist many different modalities to measure cerebral blood volume (typically measured in ml/100g, normalised by brain tissue mass similarly to perfusion) and cerebral metabolic rate of oxygen, which are not discussed here for reasons of space.

3.4 Conclusion

In this section, we have described the general anatomy and geometry of the cerebral vasculature, and then detailed the approaches to obtaining quantitative data about both the macrovasculature and microvasculature. The differences in cross-sectional areas between the two highlights the importance of the microvascular component, which has been less intensively studied. It should be noted that there does remain a noticeable 'imaging gap' between the two length scales, with very limited information available about the 'middle' vascular generations that comprise the pial circulation. However, recent advances in whole

(ex vivo) human brain imaging have opened the possibility of much more detailed parametric information becoming available, and this is a particularly exciting avenue for future study, as discussed below.

4. Cerebral blood flow models: Theory

4.0 Introduction

In this section, we consider the mathematical foundations for models of cerebral blood flow at different length scales. A schematic of the different types of models is shown in Figure 7, highlighting the many different approaches that are taken in this context. It should also be noted that these models can be coupled together, but that the coupling between the two (discussed below) is not trivial. The cerebral circulation covers a wide range of length scales, with vessel diameters ranging from around 10 μm to a few mm, as shown in Figure 8. This allows for mathematical methods based on the separation of scales to be exploited (as described below), but also means that, these models are highly computationally complex.

Before continuing, however, it should be noted that blood is well known to be a non-Newtonian fluid, with a pseudoplastic (shear-thinning) regime at low strain rates and a yield shear stress, below which the strain rate is zero. The viscosity is thus strongly dependent upon the strain rate at low values (and hence this effect is most pronounced in the smaller blood vessels). Many relationships have been used in this context to characterise the relationship between shear stress and strain rate, for example those of Casson, Cebral et al. (2002), Carreau-Yasuda, Herschel-Buckley, and Quemada, Popel and Enden (1993), with the parameters in these relationships being strongly dependent upon the blood haematocrit. The

choice of relationship has been shown to have a strong influence on some aspects of the simulated flow fields, but not others, so it is not always clear which model to select. In axisymmetric vessels with diameters less than approximately 100 μm, however, empirical relationships are commonly used, where the apparent viscosity is a function of vessel diameter and tube haematocrit; several of these have been proposed, see for example Pries et al. (1990) and Secomb and Pries (2013).

Input	Model	Output
Lumped parameters of circulatory compartments • Compartmental resistance • Compartmental compliance	Haemodynamic system model (HDSM) 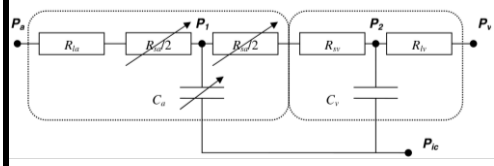	Temporal distributions: • **Pressure** • **Blood volume** • Blood flow rate
• Segment lengths • Segment diameters • Effective blood viscosity • Vessel wall properties • Boundary conditions • Initial conditions	Arterial network model (ANM) 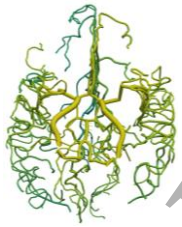	Spatial and/or temporal distributions: • **Pressure** • **Wall deformation** • Blood flow rate
• Segment lengths • Segment diameters • Effective blood viscosity • Vessel wall properties • Boundary conditions • Initial conditions	Capillary network model (CNM) 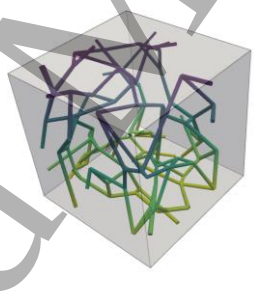	Spatial and/or temporal distributions: • **Pressure** • Blood flow rate • Wall deformation
• Vessel geometry • Effective blood viscosity • Vessel wall properties • Boundary conditions • Initial conditions	Arterial Navier-Stokes simulator (ANSS) 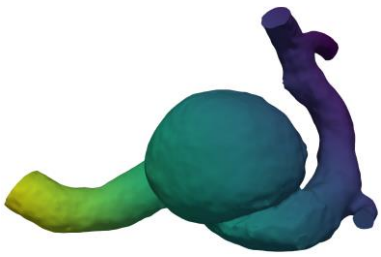	Spatial and/or temporal distributions: • **Velocity** • **Pressure** • **Wall deformation** • Wall shear stress

• Vessel geometry • Blood plasma viscosity • Blood cell properties • Boundary conditions • Initial conditions	Cell-resolved blood simulator (CRBS) 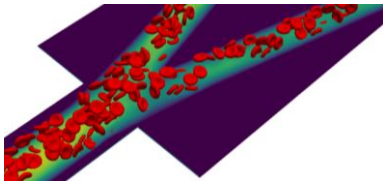	Spatial and temporal distributions: • **Velocity** • **Pressure** • **Blood cell deformation** • Effective blood viscosity
• Brain geometry • Compartmental permeabilities • Intercompartmental coupling coefficients • Mechanical tissue properties • Boundary conditions • Initial conditions	Porous (poroelastic) tissue model (P(E)TM) 	Spatial and/or temporal distributions: • **Pressure** • **Tissue deformation** • Perfusion

Figure 7 Overview of models of blood flow at different length scales. Bold font in the 'Output' column distinguishes primary variables from derived quantities.

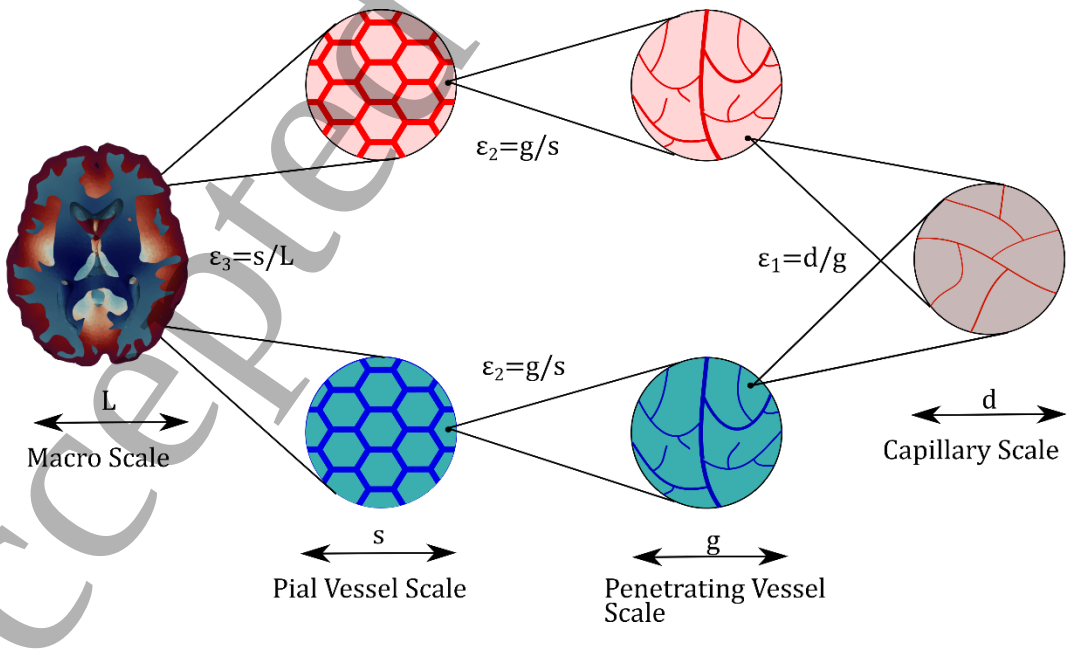

Figure 8 Schematic of different length scales and scale separation in the cerebral circulation; the parameter ε refers to the scaling between adjacent length scales as utilised in the homogenisation procedure

4.1 0D lumped parameter models

Here, only the key features of 0D models are presented because a comprehensive review on their properties and applications is provided by Shi et al. (2011). Zero-dimensional cerebral blood flow models rely on the analogy between electronic and hydraulic systems, Chappell and Payne (2020). Accordingly, the governing equations of such lumped parameter models can be derived based on an equivalent electric circuit as depicted by the HDSM model in Figure 7. To this end, a group of blood vessels is parametrised by their resistance and compliance symbolising the associated viscous losses (resistance) and blood volume changes due to vessel wall deformations (capacitance).

This approach leads to a set of ordinary differential equations which can usually be integrated using off-the-shelf computational tools once the forcing is set, for example, by defining the time-dependent cardiac output. Computations capturing potentially multiple heart cycles usually take only a few seconds with a single core CPU. Primary variables are the pressure and the blood volume as functions of time, and volumetric blood flow rate thus appears as a derived quantity. Windkessel models are the most popular members of this model family. The simplest (two-element) Windkessel model includes a resistor and a capacitor in parallel and similar systems with more than two parameters remain particularly popular. The major advantage of this approach is its ability to capture haemodynamics in multiple organs, for example describing both the pulmonary and the systemic circulations.

4.2 Models of blood flow in the macrovasculature

One-dimensional network models originate naturally from the lumped parameter description when a one-to-one mapping is established between vessel segments and the corresponding resistors and capacitances. Consequently, a graph can be used to represent the vasculature. The edges of the graph symbolise vessel segments connected at the vertices. Thereafter, governing equations can be obtained based on different assumptions. For example, it is straightforward to distinguish cases with rigid and deformable vessel walls, or steady and unsteady simulations. Choices are typically determined by the choice of the section of the vasculature under consideration.

4.2.1 Arterial Navier-Stokes simulator (ANSS)

Characterising the spatiotemporal behaviour of cerebral blood flow in detail can play an important role in certain pathologies and therapies. To this end, CFD is applied nowadays routinely to study fluid flow in specific parts of the vasculature. In this case, the governing equations are usually the incompressible continuity and Navier-Stokes momentum equations, either in steady or unsteady form. Computations tend to account for the non-Newtonian behaviour of blood using, for example, the Carreau-Yasuda model, Bardossy and Halasz (2011), Boyd et al. (2007).

The resulting partial differential equation set is typically discretised using standard techniques, such as the finite volume, finite element, or finite difference methods, Botti et al. (2018). Lattice Boltzmann methods are becoming widely used, Mazzeo and Coveney (2008) and Latt et al. (2021), because they ease the mesh-generation task based on clinical data, Kim et al.

(2010) and Zavodszky and Paal (2013). Primary variables are the velocity and the pressure fields whereas derived quantities might include the wall shear stresses relevant in pathologies, Shojima et al. (2004) and Kulcsar et al. (2011). Unsteady simulations usually incorporate multiple heart cycles to capture well-developed flow features. Such simulations can take several hours on a modern desktop using a multicore Central Processing Unit (CPU); however, simulation times can be reduced considerably using graphical processing units (GPUs), Huang et al. (2015).

Imposing realistic boundary conditions remains a major challenge. In most studies, rigid-walled blood vessels are assumed. This assumption was found reasonable in intracranial blood vessels where the surrounding tissue provides a solid embedding for the deformable vessels, Ugron et al. (2014). Nevertheless, fluid-structure interaction (FSI) simulations have been also carried out, Bazilevs et al. (2010) and Torii et al. (2008), and many of these have addressed the nonlinear hyper-elastic behaviour of the vessel wall, e.g., based on the Mooney-Rivlin or the Ogden model, Valencia et al. (2013). Regarding the inlet boundary condition, it has been demonstrated that it is necessary to add an elongated inlet segment to the region of interest to ensure well-developed flow fields, Paal et al. (2007). In addition, if tortuous vessels are located upstream of the region of interest, then at least one bend should be preserved to account for the corresponding secondary flow.

In addition to Reynolds and Womersley numbers, the Dean number is used to quantify the importance of secondary flows. Beyond inlet segment length, and curvature, the inlet profile can be also important as highlighted by both experimental and computational studies, Jansen et al. (2014). Inlet volumetric flow rate can be inferred from a haemodynamic system or an

arterial network model, Anor et al. (2010) and Ho et al. (2009). Considering the outlet boundary condition, a lumped parameter (Windkessel) model or a porous region, Ugron et al. (2014), is often connected to the outlet section(s) of the region of interest to account for downstream blood vessels. Thereafter, a constant pressure outlet boundary condition might be appropriate to characterise the venous pressure.

The Circle of Willis is of particular interest, Alnaes et al. (2007). Beyond investigations concerned with the healthy vasculature, Marshall et al. (2004) and Berg et al. (2014), an ANSS often targets intracranial aneurysms, Berg et al. (2018) and Berg et al. (2019), clipping, Kimura et al. (2009), stenting, Janiga et al. (2015), stenoses, Zhang et al. (2013) and Beratlis et al. (2005), and blood clot formation, Ouared and Chopard (2005). Thanks to comprehensive clinical datasets and a generic effort to develop automated pipelines, Villa-Uriol et al. (2011) and Sarrami-Foroushani et al. (2021), patient-specific geometries are gaining popularity whereas artificial geometries are often considered to improve understanding of fundamental flow features, Paal et al. (2007). Simulations have now been validated extensively against well-controlled experiments including phantoms, Ugron et al. (2011), and clinical measurements, Berg et al. (2014) and Cebral et al. (2009).

4.2.2 Arterial network model (ANM)

In the second case, the time-dependence of the flow at time scales of around 1 Hz is explicitly considered, but the spatial information is reduced to a 1D model. The governing equations (based on continuity and momentum) are well-established and normally written in terms of the local flow rate, $Q(x,t)$, and vessel cross-sectional area, $A(x,t)$:

$$\frac{\partial A}{\partial t} + \frac{\partial Q}{\partial x} = 0$$

$$\frac{\partial Q}{\partial t} + \frac{\partial}{\partial x}\left(\left[\frac{\gamma+2}{\gamma+1}\right]\frac{Q^2}{A}\right) + \frac{A}{\rho}\frac{\partial p}{\partial x} = -2\pi(\gamma+2)\upsilon\frac{Q}{A}$$

where the flow rate is equal to the product of the vessel cross-sectional area and the area-averaged velocity, U. Blood is taken to have density ρ and kinematic viscosity υ. The 'correction term' in the convection term compensates for the fact that the area-averaged momentum term is different from the momentum calculated based on the area-averaged velocity (since the velocity profile is not flat). The parameter γ is the exponent in the assumed power law profile for the velocity field.

To 'close the loop', a relationship between blood pressure, p, and vessel cross-sectional area is normally applied that models the mechanical response of the vessel wall. Although the vessel wall can be considered as a viscoelastic material, in the context of the cerebral circulation, it is much more common to assume a purely elastic material and to formulate this relationship based on the 'independent ring' model. The presence of waves in the flow field and the presence of vessel nodes means that travelling waves generate reflections: complex wave forms can be generated that encode information about the geometrical and structural properties of the network. It should be noted that the number of pressure-area relationships proposed is very large and that there is thus a wide variety of forms that have been adopted, see for example Payne (2017), although the 'independent ring' model is the most popular in the context of the cerebral circulation.

This dynamic 1D approach has been widely applied to the whole of the circulation, with highly accurate models developed. It has also been applied to the cerebral circulation in the large

vessels, see for example Alastruey et al. (2007), although in these cases the microcirculation (and downstream circulation) is normally modelled via the use of three-element lumped parameter (i.e., Windkessel) circuits. More recently, it has been used together with a reconstruction algorithm to infer optimal blood flow distributions across the visible part of the arterial network based on partial data, Park et al. (2020).

An alternative dynamic approach to the blood flow in large vessels is based on the formulation proposed by Womersley (1955), where a sinusoidal driving pressure is applied to a rigid, axisymmetric vessel (where the convection term is neglected). The resulting flow rate is then given (in the frequency, ω, domain) by:

$$\hat{Q} = \frac{\hat{p}\pi R^2}{i\omega\rho}\left\{1 - \frac{2}{\alpha i^{3/2}}\frac{J_1(\alpha i^{3/2})}{J_0(\alpha i^{3/2})}\right\}$$

where the overhat denotes that the variable is in the frequency domain and $\alpha = R\sqrt{\frac{\omega}{\nu}}$ is the Womersley number. The Womersley number is a measure of the importance of the dynamic term relative to the inertia term and decreases monotonically as the flow passes towards the smallest vessels, meaning that the flow behaviour changes as the length scale changes.

This formulation can be used to replace the momentum equation, and this approach has been extended to develop 1D models of flow in compliant vessels, using a wave equation type approach. Flores et al. (2016) have shown that the use of the Womersley formulation, coupled with the continuity equation and a tube law, leads to an equation of the form:

$$\frac{\partial^2 \hat{p}}{\partial x^2} = (i\omega Z' C')\hat{p}$$

where the vessel has resistance per unit length of Z' and compliance per unit length of C'. This can be solved with suitable boundary conditions to provide a matrix-style relationship between inlet and outlet conditions, and then applied to a network of vessels to yield a dynamic equivalent to the steady state pure resistance formulation. Since the relationship between pressure and flow is linear, the equations can be formulated in matrix form (assuming conservation of mass and continuity of static pressure) and the flow field easily calculated. The computational cost then primarily arises in inverse-transforming the solution back into the time domain. This has been shown to be in good agreement with full 3D models of blood flow in compliant arterial networks, indicating that it is a computationally inexpensive method for solving a dynamic 1D network flow.

This methodology was extended further to consider the case when the parameter $\alpha i^{3/2}$ is small, using a perturbation method approach, Payne and El-Bouri (2018). This provided a justification for when the advection term can be neglected, a first order differential equation approximation for the flow-pressure relationship, a justification for when blood volume can be modelled as quasi-steady-state, and when the difference between assuming conservation of static pressure or total pressure at vessel nodes is negligible. Essentially, all four approximations are valid in vessels of diameter < 1 mm, enabling the governing equations to be considerably simplified in the microcirculation (as described below).

4.3 Models of blood flow in the microvasculature

Physiologically realistic models of the cerebral microcirculation essentially first became available in 2006, as a result of new data sets, both ex vivo and in vivo, from the pioneering studies of Cassot et al. (2006), Lauwers et al. (2008), and Lorthois et al. (2011). This led to a

significant number of new studies and by 2013, Linninger et al. (2013) were able to describe 16 studies into the cerebral microcirculation, with a mixture of human and animal models, both 2D and 3D simulations, steady and dynamic simulations, and network sizes up to over 350,000 vessels. More recently, Payne and El-Bouri (2018), provided an updated summary of these models and there have been many more since. A summary of the different microvascular models available is provided below, following the list given in Table 2.

4.3.1 Cell-resolved blood simulator (CRBS)

There are numerous models of the microvasculature at different scales. On the smallest scale, simulations of flows of individual RBCs and platelets are possible in cell-resolved simulations. The rapid growth of computational power has led to several recent studies that aim to simulate the transport of individual RBC through simple geometries. These resource-intensive multi-physics simulations couple the mechanical responses of RBCs, white blood cells and platelets with the fluid dynamics of the plasma flow.

Cell-resolved simulations consider blood as a suspension of particles – including typically red blood cells, and platelets – in blood plasma (matrix fluid), Fedosov et al. (2011). Blood plasma is typically described as a Newtonian fluid governed by the incompressible Navier-Stokes momentum equations which can be simplified to the unsteady Stokes equations because of the low Reynolds number (creeping flow dominated by viscous effects), Balogh and Bagchi (2017). Blood cells are discretized using a surface representation with their deformation captured by a membrane deformation equation. Cell shapes and mechanical properties are deduced from microscopy, Fung et al. (1981) and Li et al. (2012). Several mechanical models of RBCs have been proposed, for example the spectrin-link membrane model, Li et al. (2005),

and the energy model, Skalak (1973). Primary variables are the fluid velocity and pressure fields and the solid deformation field whereas derived quantities of interest might include the apparent fluid viscosity and the haematocrit. Input parameters are the computational domain and blood cell shapes (geometry), and the material properties of the plasma and the blood cells.

The fluid equations are usually approximated by the lattice Boltzmann method, MacMeccan et al. (2009), but finite-volume/spectral solvers have been also utilised, Balogh and Bagchi (2017). Both mass-spring-damper systems, Zavodszky et al. (2017) and finite element models, Kotsalos et al. (2021) are popular choices to capture membrane deformations caused by fluid pressure and shear stresses. Fluid-solid coupling is typically established by the immersed boundary method. The computational cost of the corresponding simulations varies in a wide range depending primarily on the number of the modelled blood cells, Alowayyed et al. (2018). Whereas simulations with a small number of RBCs are feasible on newer multi-core desktops, describing blood flow with about 10,000 RBCs can require computations lasting for multiple days using hundreds of computer cores. Long time-integration is necessary to reach a statistical steady state and a sufficient sample size for averaging. A review of the corresponding numerical methods is provided by Ju et al. (2015).

To date, geometries of interest have been restricted to microscale bifurcations, Bernabeu et al. (2020) and Enjalbert et al. (2021), capillary networks, Ebrahimi and Bagchi (2022), micro-aneurysms, Czaja et al. (2022), and porous media, Zhou et al. (2022). Simulations pointed out the limitations of empirical plasma-skimming models, Enjalbert et al. (2021), and led to the creation of an advection-diffusion model of haematocrit transport, Zavodszky et al. (2017).

Furthermore, computations provide insights into how haemorheology is influenced by diseases, such as malaria, Navidbakhsh and Rezazadeh (2012), sickle cell disease and diabetes, Hashemi and Rahnama (2016) and into the mechanisms of thrombosis, Chopard et al. (2017). Simulations have been validated using microfluidics experiments, van Rooij et al. (2021) and Zhou et al. (2022). These models open the possibility of simulating both the effective viscosity and haematocrit splitting effects, providing further insight into the details of the flow at this length scale, as well as being invaluable in the study of thrombosis and thrombolysis, Mehrabadi et al. (2016) and Belyaev (2018).

On a coarser level, treating RBCs effectively as rigid particles, several studies have been performed that simulate the transport of individual cells within microvascular networks, see for example Schmid et al. (2017) and Hartung et al. (2018). These models have shown strong depth-dependence between the cortical layers and analysis of the pathways through the capillary bed have shown that there are preferred pathways, indicating that the flow field is not purely a function of the geometry of the network but also a function of the haemodynamic relationships (and hence that regulation of flow is likely to be different at different levels), Hartung et al. (2018). These models are heavily dependent upon the choice of haematocrit splitting rules at junctions but have shown that the variability of haematocrit within these networks is very significant, although at length scales of more than approximately 100 μm, the effects on permeability have been shown to be quite small, indicating that this effect is only significant at relatively small length scales.

4.3.2 Capillary network models (CNM)

At a scale above cell-resolved simulations lies what can be termed the capillary network model. At this scale, blood is treated as a continuum fluid despite the plug flow characteristics of RBCs flowing through capillary vessels, Pries and Secomb (2003). Due to the laminar nature of blood flow in the microcirculation, a linearisation of the Navier-Stokes equations is used to simulate the blood flow (Stokes flow). This is often simplified to Poiseuille flow which treats the vessel as a resistance to flow, with this resistance dependent on the viscosity of the blood, length, and diameter of the vessel:

$$R = \frac{\Delta p}{Q} = \frac{128\mu L}{\pi D^4}$$

where the flow rate, Q, is linearly related to the pressure drop, Δp, as a function of the vessel diameter D and length L, and dynamic blood viscosity μ. This equation is, however, strictly only valid for a steady, Newtonian fluid in a rigid, axisymmetric vessel. At this scale the walls of the microvessels are generally considered rigid due to the lack of smooth muscle cell surrounding the vessels. The Poiseuille equation thus provides a very good first order estimate for most vessels, although care must be taken when considering vessels with significant tortuosity, as the resistance to flow can increase rapidly, Mohktarudin et al. (2022), and this can have implications for thrombectomy, Mokin et al. (2020). The tortuosity of blood vessels has been shown to be higher in vascular networks in stroke patients when compared to age-matched healthy controls, Deshpande et al. (2021), so this is an important consideration.

A key feature of the simulation of flow in the microcirculation is the strong dependence of viscosity on the dimensions of the vessel and the haematocrit due to the Fahraeus-Lindqvist

effect. This has resulted in several empirical relationships for viscosity in axisymmetric vessels, see for example Pries et al. (1990), Pries et al. (1992), Pries et al. (1996), and Pries and Secomb (2005). There is some divergence of values between the different relationships, which means that this remains an area in which more experimental data are required.

As well as the empirical relationships for the apparent viscosity of flow in small vessels (diameter less than approximately 100 μm), relationships based on experimental data have been proposed for haematocrit splitting at bifurcations. This is because at bifurcations the division of red blood cells is not the same as the division of blood flow (hence the haematocrit values in child vessels are not equal to that in the parent vessel). Since changes in haematocrit also affect the viscosity of the flow, the flow patterns and haematocrit distributions can thus be complicated in interconnected networks and iterative methods must be used to calculate the flow field. Models for this splitting have been proposed by Pries et al. (1990) and Gould and Linninger (2015), although no systematic approach has yet been carried out to explore the range of validity of these models and to compare them with more detailed models of vessel junctions. Alternatively, two-phase flow models that explicitly mimic the flow field as a red blood cell rich inner layer and a plasma outer layer have been proposed and shown to fit well with experimental data, Sharan and Popel (2001).

Modelling approaches for the microvascular networks then fall into two types, based on either a real or a reconstructed network. The former has the advantage of being based on a true network (but is then limited by the field of view of the available image, which is often relatively small) and the latter has the advantage of scalability (but is limited by the accuracy of the reconstruction algorithm). Most studies have adopted the former approach, but it

should be noted that the choice of boundary conditions strongly influences the flow field that is calculated, Lorthois et al. (2011); this can be done either by setting Dirichlet / Neumann boundary conditions on the surface nodes, or by optimising the flow field to match target values of pressure and shear stress within the network, see for example Sweeney et al. (2018).

Issues with accurate segmentation have promoted the alternative methodology of generating artificial statistical networks to match experimental measured properties. The advantage of this approach is that it can be scaled up to arbitrary dimension and that it can be characterised in terms of a permeability tensor (and hence scaled up to even larger length scales). Other authors have developed regular bifurcating networks, see for example Boas et al. (2008) and Payne and Lucas (2018), which provide a simplified representation that can easily be used for simulations of the vasculature response to stimuli, but as these contain no spatial information they are best used as test beds for more complex models.

Accurate microvascular models open the possibility of calculating transit time distributions based on network properties, Park and Payne (2013) and Goirand et al. (2021), and fast and slow pathways have been identified, where local blockages only affect the slow pathways but global changes in pressure affect both pathways equally. Several studies have been performed to consider capillary transit time heterogeneity (CTH), see for example Jespersen and Ostergaard (2012) and Ostergaard et al. (2014) and this has been shown to impact oxygen extraction fraction (OEF), although this remains relatively poorly understood. As transit time distributions can be estimated from imaging data via residue functions, this is a promising way of gaining additional information about the microcirculation (although the estimation of these distributions from noisy under-sampled time series remains challenging).

However, if the aim is to simulate large regions of the brain, for example a whole lobe or the entire cortex, then simulations of individual microvessels become computationally intractable. Although an entire mouse brain vasculature has recently been simulated based on high-resolution imaging of individual animals together with synthetic networks to cover the whole range of length scales, Linninger et al. (2019) and Hartung et al. (2021), providing significant insight into the flow distributions in a highly complex network, this is substantially smaller than a human brain. A different method to simulate large regions of blood flow is thus required due both to the lack of computational power and the lack of anatomical information about the microvasculature.

4.3.3 Porous (poroelastic) tissue model P(E)TM

In the poroelastic framework, vessels embedded in a deformable tissue matrix are grouped to describe internal blood (cerebrospinal and interstitial fluid) flows. This method moves from simulating individual microvessels to describing flow through the entire cerebral microcirculation. Once relatively small deformations are assumed compared to the size of the domain of interest, the theoretical connection between the underlying Cauchy momentum equations (including both fluid and solid motions) and the poroelastic formulation is provided by homogenisation or volume-averaging, Shipley and Chapman (2010), Shipley et al. (2020), El-Bouri and Payne (2015).

The Navier-Stokes equations for these networks can thus be reduced to the form of a porous medium approximation:

$$\mathbf{u} = -\mathbf{K}\nabla p$$

where the properties of the network are summarised within a permeability tensor, $\mathbf{K}$, relating the flow field, $\mathbf{u}$, to the pressure field, p, see for example Shipley and Chapman (2010) and El-Bouri and Payne (2015).

Separating the deformable parenchyma (brain tissue) from the blood-filled lumen and the interstitial and cerebrospinal fluid spaces then leads to a generalised multiple network poroelasticity formulation. Both unsteady and steady poroelastic models have been considered and simplified multi-compartmental porous models have been also introduced. In fluid compartments, the permeability tensor, viscosity, compressibility, and Biot parameters link the strain field to the pressure and fluid velocity fields.

This result can be applied to simulate flow in the microvasculature using any arbitrary number of compartments e.g., capillary bed, arterioles, venules. The velocity in each compartment can be calculated via the porous medium approximation and the governing equation for a porous medium can be applied, i.e.:

$$\phi_j = \alpha_j \varepsilon + \frac{p_j}{Q_j}$$

where each individual phase has Biot-Willis coefficient α_j and specific storage Q_j. The volumetric strain is finally related to tissue displacement $\mathbf{w}$ via:

$$\varepsilon = \nabla . \mathbf{w}$$

We illustrate this model by assuming that the microcirculation can be simplified to three blood compartments, as this has been the most common choice. Multiple blood compartments are created by grouping blood vessels based on their diameter or the structure

of the vessel wall, although there is no rigorous definition or general agreement on how this is best done, so methods remain somewhat ad hoc in nature.

Conservation of mass, assuming an incompressible fluid, in an Eulerian co-ordinate system then gives:

$$\frac{\partial}{\partial t}\left(\alpha_a \varepsilon + \frac{p_a}{Q_a}\right) - \nabla.(\mathbf{K}_a \nabla p_a) = -\beta_{ac}(p_a - p_c)$$

$$\frac{\partial}{\partial t}\left(\alpha_c \varepsilon + \frac{p_c}{Q_c}\right) - \nabla.(\mathbf{K}_c \nabla p_c) = \beta_{ac}(p_a - p_c) - \beta_{cv}(p_c - p_v)$$

$$\frac{\partial}{\partial t}\left(\alpha_v \varepsilon + \frac{p_v}{Q_v}\right) - \nabla.(\mathbf{K}_v \nabla p_v) = \beta_{cv}(p_c - p_v)$$

where the subscripts *a*, *c*, and *v* refer to the arterial, capillary, and venous compartments respectively, each of which has pressure p_i and blood velocity $\mathbf{u}_i$, all of which are functions of space and time. The sum of the volume occupancy fractions is equal to the blood volume fraction (which can be directly related to measurements of cerebral blood volume, as discussed earlier).

The flow between the different compartments is governed by the coupling coefficients, β_{ij}, which govern the rate of flow from compartment *i* to compartment *j*; it is normally assumed that there is a linear relationship between the pressures in the two compartments and the flux. It should be noted that most mathematical models of CBF in the microvasculature also assume that the volume fraction is constant, although this remains to be fully validated.

In the solid compartment, a constitutive law establishes the stress-strain relationship, typically based on the Young's modulus and Poisson's ratio of the tissue. Computational

approaches tend either explicitly consider tissue displacement (for example, as they wish to examine the effects of post-ischaemic swelling, where there can be significant movement of brain tissue) or to neglect it. In the former case, a constitutive model for the tissue must be assumed; although we will not have space to consider this in any detail here, we note that the simplest model, i.e., that of a linear, elastic, isotropic material, can be applied via:

$$G\nabla^2\mathbf{w} + \left(\frac{G}{1-2\nu}\right)\nabla(\nabla.\mathbf{w}) - \sum_j \alpha_j \nabla.p_j\,\mathbf{I} = \rho_s\frac{\partial^2\mathbf{w}}{\partial t^2}$$

where the tissue has density ρ_s, shear modulus G, and Poisson ratio ν. Note that other authors sometimes also include additional terms to account for the acceleration of the fluid inside the solid matrix, but these terms are negligible except at very high frequencies and can thus nearly always be neglected in this context. Even the acceleration term on the RHS of the equation above is generally found to be small.

The governing equations are typically solved by the finite element method, but finite volume simulations have been also reported. Steady state results can be obtained using a multi-core desktop within minutes whereas unsteady simulations can take much longer depending primarily on the time window of interest. Derived quantities of interest might be the midline shift of the brain caused by large deformations or perfusion, Mokhtarudin and Payne (2017) and Chou et al. (2016). Previously, several pathologies have been considered using this modelling framework, such as Alzheimer's disease, Guo et al. (2018) and Vardakis et al. (2020), hydrocephalus, Chou et al. (2016), oedema, Vardakis et al. (2016) and Mokhtarudin and Payne (2017), and acute ischaemic stroke, Jozsa et al. (2021). Validation of the resulting deformation and velocity fields is an ongoing effort. Simulations show promising agreement with perfusion-weighted images, phase-contrast imaging, and deformations quantified based on

non-contrast computed tomography, Vardakis et al. (2019) and Mokhtarudin and Payne (2017), although further detailed studies are still required for full validation.

4.4 Coupling models of blood flow

The modelling frameworks adopted for various length scales are clearly very different and coupling them together is a non-trivial task. Since it is not possible to simulate every blood vessel individually, in any whole brain model a division must be made at some length scale between a continuum approach and a discrete approach. This is normally either done at the arteriole-capillary boundary (typically when examining models at the length scale of a single voxel), see for example El-Bouri and Payne (2016), or at the cortical surface (typically when simulating the whole brain), see for example Jozsa et al. (2021). Models of the pial circulation have been limited by the lack of available experimental data regarding their anatomy and geometry, which also makes the coupling challenging.

The key difficulty in coupling a continuum model with a discrete model in this context is that the flow from or to the discrete vessels introduces a singularity in the governing equations for the continuum (essentially because this flow appears as a point source or point sink). A means of 'spreading' these terms out spatially needs to be adopted within the confines of the discretisation of the space that is typically used in solving the governing equations within the continuum phase. One rigorous way of doing this was proposed by Peyrounette et al. (2018), based on analytical approximations of the pressure field in the vicinity of the coupling points that enable continuum solutions to be considered.

At a whole brain model, the procedure proposed by Padmos et al. (2021) and extended by Jozsa et al. (2021) is based on the estimation of perfusion territories, as shown in Figure 9. Flow from the large vessels is then distributed across the relevant perfusion territories to ensure approximately constant perfusion across the territories, essentially mimicking the pial circulation. This highly simplified approach enables whole brain models to be run without very high computational expense and allows for the inclusion of information about the collateral circulation (about which imaging data can be acquired), Padmos et al. (2021).

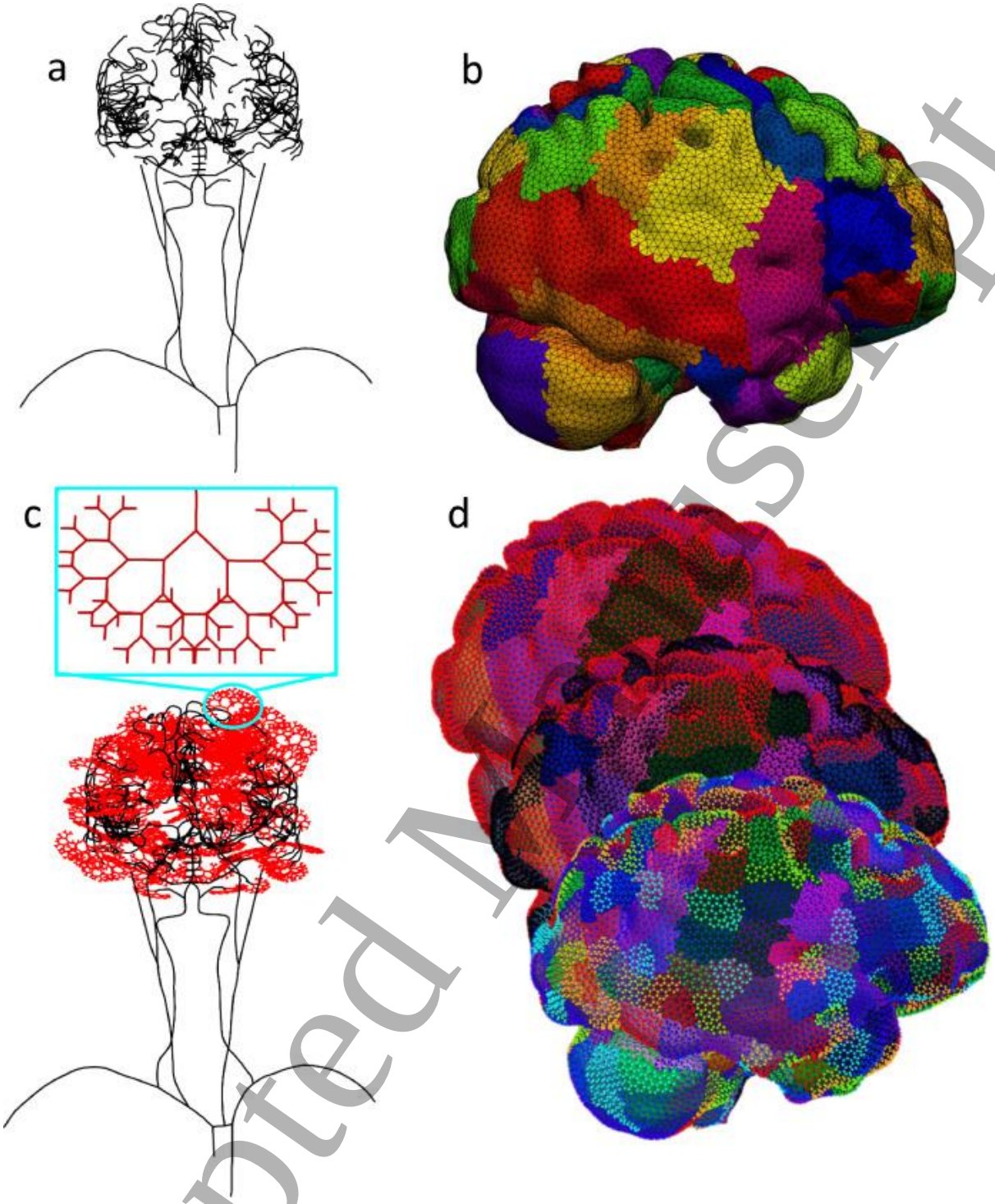

Figure 9 "(a) The large arteries used in the model, starting at the heart and ending at the major cerebral arteries. (b) The surface mapping on the surface of the brain. Each colour denotes the perfusion territory of a single outlet of the large arteries in (a). Shown is the right side of the brain. (c) At the outlets of the large cerebral arteries in (a), a bifurcating tree is generated. (d) The bifurcating trees are mapped on the surface by iterative division of the

perfusion territories in (b). Shown is the right side of the brain." Figure and legend reproduced with permission from Padmos et al. (2021).

4.5 Conclusion

In this section, we have examined the mathematical foundations for models of cerebral blood flow. These have been divided into approaches for the macrovasculature and the microvasculature for convenience, as they have followed very different paths in model development. The coupling of these models together has also been considered briefly, although this is a challenging mathematical problem that has only been tackled by a few authors. In the next section, we consider the implementation of these models.

5. In silico clinical trials

5.0 Introduction

In this section, we consider the use of models of CBF in in silico clinical trials of stroke and aneurysms, both the development of the disease and the interventions made to treat it. This is because, to the authors knowledge, in silico trials have only been attempted for ischaemic stroke and aneurysms. Other conditions related to CBF, for example dementia and traumatic brain injury, have been much less studied in this context, although the work presented here would have obvious applications in these other clinical conditions where the role of CBF in disease progression is now increasingly appreciated, see for example de la Torre (2018), Rius-Perez et al. (2018) and Scheffer et al. (2021). It should also be carefully noted that the choice of model is very much guided by the specific application of the model, with different models (and different accuracies) being appropriate for different situations.

5.1 Methodology

Recently, both the European Parliament and the United States Congress have drawn attention to the potential benefits of employing computational models in medical device and drug development. An in silico clinical trial builds on computational models to evaluate the safety and efficacy of therapies and treatments. An in silico trial thus "simulates a disease and its corresponding therapies on a cohort of virtual patients to support the development and evaluation of medical devices, drugs, and treatment", Miller et al. (2021). These have the potential to reduce significantly the time and cost of clinical trials, helping to avoid clinical trial failure and to support clinical trials for diseases with low prevalence.

Models of cerebral blood flow are now becoming sufficiently mature to estimate the impact of clinical operations on physiological variables. Haemodynamic variables, such as brain perfusion, play an important role in patients' health and thus simulations can be suitable to estimate how patient cohorts, and eventually individuals, would react to a specific treatment. These trials do not yet attempt to mimic individual (patient-specific) subjects, rather they aim to provide an accurate statistical representation of the population being studied. This enables studies to be performed in a similar manner to a clinical trial. For more information about in silico trials, see Viceconti and Hunter (2016).

A virtual patient is a set of models and parameters determined by the medical device or drug of interest. In the context of cerebral blood flow, a virtual patient relies on one or more of the models described above, and the input parameters such as viscosity, vessel wall stiffness etc. Thanks to advances in clinical measurement techniques, it is nowadays possible to infer some

of these parameters in a patient-specific manner. Conceptually, such “one-to-one mirroring” is the most straightforward method to obtain virtual patients. For example, an individual’s blood viscosity can be measured from a blood sample, and the stiffness of a blood vessel segment can be estimated using magnetic resonance imaging. However, the choice of parameter values remains one of the most challenging aspects of any physiological model. Both mathematical and computational approaches will be needed to constrain the parameter space to a reasonable size.

Therefore, the concept of ‘patient-specific simulations’ is now starting to be considered and such computations might be part of an individual's digital twin covering an individual’s most relevant pathophysiological behaviour. It is important to acknowledge though that, strictly speaking, patient-specific simulations have *not* been carried out yet, Steinman and Pereira (2019), and numerical investigations to date have been limited to integrating *some* patient specific parameters, such as the computational geometry inferred from angiography. Inferring the comprehensive set of input parameters for cerebral blood flow models is an unresolved challenge. For example, in the case of arterial Navier-Stokes simulators, difficulties associated with absolute pressure measurements undermine the patient-specific treatment of boundary conditions. Although patient-specific cerebral haemodynamic simulations might become possible in the future, until then another approach is needed to determine parameters for virtual patients. To date, in silico trials have inferred the necessary parameters from different patient cohorts and merged them for simulations based on statistical models. This approach might be referred to as chimerisation and allows the user to exploit information available from different sources.

It should be noted that the uncertainty present in the details of the model means that the demonstration of model credibility to regulatory bodies and clinical organisations will be critical in translating these models into routine clinical practice. Amongst other aspects of this are reproducibility, replicability, verification, and validation, see for example Mulugeta et al. (2018). The recent VVUQ protocols provide a basis for starting these processes. Techniques such as sensitivity analysis will also be an important aspect of this process.

5.2 Acute ischaemic stroke

One of two in silico trials related to cerebral blood flow is described in Miller et al. (2021), where patients with large vessel occlusion acute ischaemic stroke who were eligible for mechanical thrombectomy were considered. The MR CLEAN registry, Berkhemer et al. (2015), was used within the INSIST project, Konduri et al. (2020), to generate a model to predict brain injury and stroke treatment in terms of a statistical clinical outcome model. The authors note that the study is a “proof of concept” at this stage, following on from other studies in other body organs such as the coronary circulation, Chiastra et al. (2019).

Early models of thrombolysis focused on the biochemical processes, considering idealised geometries, see for example Anand and Diamond (1996), Wootton et al. (2002), Pleydell et al. (2002) and Bannish et al. (2014). These models link kinetic compartmental models of molecules such as plasminogen, plasmin, fibrinogen and antiplasmin, with transport equations for these molecules through the clot; for a review of these see Fogelson and Neeves (2015). More recent work has expanded these models to patient-specific geometries, Piebalgs et al. (2018), Gu et al. (2019) and Gu et al. (2022), with one study combining both thrombolysis and thrombectomy in one patient-specific geometry, Manchester et al. (2021).

For thrombectomy, several additional computational models are required to simulate both the mechanical properties of the clot and the interaction between the clot and the device (of which there are now a number, see for example Chueh et al. (2021), Kuhn et al. (2020) and Ospel et al. (2019)). Recent studies of mechanical thrombectomy include those by Chueh et al. (2017), Talayero et al. (2019), Weafer et al. (2019), Madjidyar et al. (2020) and Mousavi et al. (2021), investigating the performances of different retrievers both experimentally (in vascular replicas) and computationally in response to clots of varying mechanical properties.

Mechanical testing of clot analogues (i.e., clots prepared from blood mixtures of varying haematocrit) has shown that the mechanical behaviour is strongly dependent upon the clot composition with the microstructure of the clot also a function of age. A hyper-viscoelastic constitutive model is suitable to capture the mechanical behaviour, Johnson et al. (2021), and this has recently been implemented in models using simplified geometries to provide accurate predictions of the clot deformed shape, Fereidoonnezhad et al. (2021) and Fereidoonnezhad and McGarry (2022).

These models have now been implemented within the first patient-specific simulations of mechanical thrombectomy using a stent-retriever, Luraghi et al. (2021a) and Luraghi et al. (2021b), Figure 10. This also included a study of the risk of clot fragmentation during mechanical thrombectomy using a damage initiation criterion based on Fereidoonnezhad et al. (2021). Fragmentation is a significant risk in this procedure, as it can lead to a ‘shower’ of microthrombi passing into the downstream circulation and preventing reperfusion; this has previously been considered in models of perfusion, El-Bouri et al. (2021), and the mechanical

properties of the clot have been shown to affect the change in permeability of the downstream circulation. It is worth noting that the prediction agreed with the clinical observation that the clot remained intact and was not removed on the first attempt.

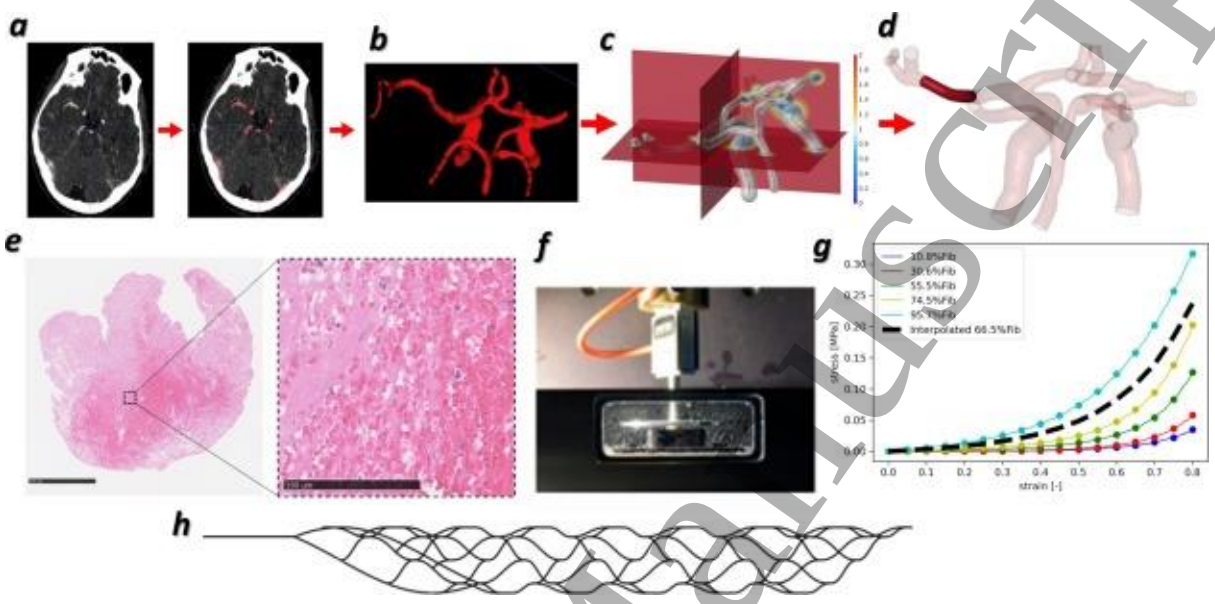

Figure 10 "(a) CT images are segmented to extract the (b) intracranial arteries. (c) Centerlines are processed, and the vessel surface meshes are derived with the aid of a levelset image. (d) Clot location is visible in the transparent representation. (e) Hematoxylin and Eosin histological staining of a clot tested to derive mechanical properties from (f) unconfined compression tests. (g) With increasing fibrin/platelet content, the clot stiffness increases. The stress–strain curve for the patient-specific clot considered in this study (black dotted line) was obtained by interpolating the known curves. (h) Model of the stent-retriever." Figure and legend reproduced with permission from Luraghi et al. (2021a).

These new models of thrombectomy thus have great potential predicting the displacement and movement of clots, although given the variability in their properties, which are unlikely to be known in advance of the intervention, there is considerable uncertainty in any

prediction (and thus in the optimal choice of device); this remains an area requiring further investigation, to determine the amount of information required to decide on the intervention. The event-based in silico trial pipeline reported by Miller et al. (2021) uses ANM and PETM together to quantify how both successful and unsuccessful stroke treatments impact blood flow both in the macrocirculation and the microcirculation. Thereafter, a statistical model predicts patients' functional outcome based on the location and size of brain territories with low perfusion.

5.3 Cerebral aneurysms

Simulations of the treatment of aneurysms have a much more substantial track record than the treatment of ischaemic stroke. There now exist substantial databases of clinical and imaging data from patients with both ruptured and unruptured aneurysms, for example through the @neurIST project (with nearly 500 patients); for full details of the processing toolchain, see Bogunovic et al. (2011) and Villa-Uriol et al. (2011). These provide populations from which virtual populations can be reconstructed and studies performed to quantify the effects of parameters such as hypertension and hypotension, Sarrami-Foroushani et al. (2015).

Likewise, virtual models of devices, including coils and flow diverters, have been developed, see for example Larrabide et al. (2012) and Shapiro et al. (2013) that can be included within the simulations to quantify the changes in the haemodynamics in and around the aneurysm caused by the intervention, see for example Jeong and Rhee (2012) Goubergrits et al. (2014), Mut et al. (2014), Peach et al. (2019) and Tikhvinskii et al. (2022). Multiple parameters, including wall shear stress and pressure can be calculated, although it is worth noting that

many assumptions must be made about the haemodynamic environment and the wall properties, as described earlier.

A schematic of the pipeline that is used in this context is shown in Figure 11 also highlighting the uncertainty in the model outputs that play an important part in decision making. In this context, the coupling between high-fidelity 3D models and 0D Windkessel models is of particular importance. This particular in silico trial was thus based on modelling the treatment of intracranial aneurysms using flow diverters (the FD-PASS study), and this showed good agreement with values reported in three clinical trials, Sarrami-Foroushani et al. (2021). The pipeline aimed to evaluate the efficacy of flow diverters based on the flow field and clot formation in the aneurysm sac.

This trial opens two possibilities for modelling the cerebral vasculature: patient-specific models, which are directly constructed based on an individual patient's imaging data, and population-based models, which are constructed based on all available data. At present, there are no clear guidelines about which is the preferred approach, although multiple factors must be taken into consideration here, including the quality of the available patient data relative to the population-based data. It is likely that in future both approaches will be used in separate contexts. In the same manner as for randomised clinical trials, power calculations must be performed to calculate the size of the virtual population to identify a given type I error, see for example the calculation in Sarrami-Foroushani et al. (2021).

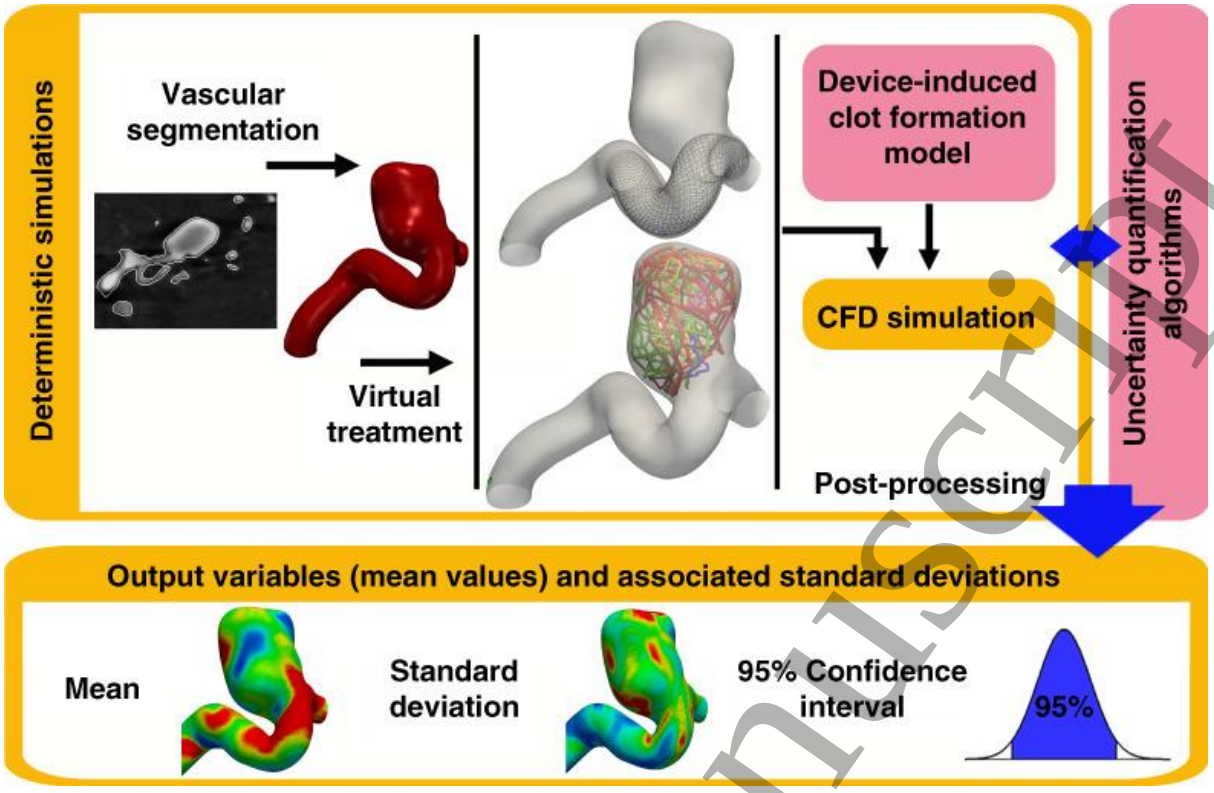

Figure 11 Schematic of simulation of cerebral aneurysm and resulting outputs, reproduced with permission from Sarrani-Foroushani et al. (2017)

5.4 Conclusion

In this section, we have examined computational models that aim to simulate pathological conditions that involve CBF. Although the models of aneurysms and their treatment are now relatively well-established, those of ischaemic stroke and its treatment are much earlier in their development with only very recent successful attempts to simulate interventions. In both cases, the potential for examining the differing outcomes of alternative interventions and therapies via a computational model in advance of treatment is clear, although it should be noted that the clinical timescales in these two cases are very different. It is also worth noting that there are many confounding factors (such as age) that have yet to be included

within these models. These are, however, very promising avenues for future studies, as will be discussed briefly in the final section below.

6. Conclusions

In this review, we have considered the modelling of CBF, both the theory behind these models and the practical implementation. The last fifteen years have seen a considerable amount of work carried out to model the cerebral vasculature with much greater accuracy, although much work remains to be done to improve our understanding of this highly complicated network, both in terms of its anatomy and geometry and its active behaviour. The transition towards the development of in silico trials however opens the possibility of providing a much better understanding of different cerebral pathologies and the appropriate interventions.

The computational frameworks for pathological cerebral conditions that are being developed here also provide opportunities for simulating other aspects of the cerebral circulation. Some work has been performed on modelling the transport of oxygen through the cerebral vasculature at multiple length scales, although this is still in need of detailed validation, which is a highly challenging task. These models can also be used to simulate the transport of contrast agents (to help to improve our understanding of medical imaging techniques) and pharmaceutical interventions (to help to improve our understanding of drug delivery to the brain, a notoriously difficult technical problem).

The major limitation on all models of the cerebral circulation however remains the lack of high-quality experimental data, both anatomical data about the different generations of the

vasculature, and geometrical and mechanical properties of the blood vessels. Similar difficulties exist in mechanical models of brain tissue, emphasising the need for improved measurement techniques and more innovative methods to extract information from data sets. There has been an increase in the use of machine learning techniques in other fluid dynamics contexts, and the potential for these to add value in understanding and simulating CBF could be significant.

Acknowledgements

SJP would like to thank many individuals over many years who have provided thoughtful insight into the cerebral circulation. SJP is supported by a Yushan Fellowship from the Ministry of Education, Taiwan (# 111V1004-2).

TIJ is supported by a Career Bridging Fellowship provided by Amsterdam University Medical Centres. TIJ and WKEB received funding from the European Union's Horizon 2020 research and innovation programme, the INSIST project, under grant agreement no. 777072.

WKEB has received funding from the Royal Society Research Grant scheme, grant no. RGS\R1\221149.

References

Aaslid R, Markwalder TM, Nornes H. Noninvasive transcranial Doppler ultrasound recording of flow velocity in basal cerebral arteries. J Neurosurg. 1982 Dec;57(6):769-74.

Abbott NJ, Patabendige AA, Dolman DE, Yusof SR, Begley DJ. Structure and function of the blood-brain barrier. Neurobiol Dis. 2010 Jan;37(1):13-25. doi: 10.1016/j.nbd.2009.07.030. Epub 2009 Aug 5.

Agoston DV. How to Translate Time? The Temporal Aspect of Human and Rodent Biology. Front Neurol. 2017 Mar 17;8:92. doi: 10.3389/fneur.2017.00092. eCollection 2017.

Ainslie PN, Cotter JD, George KP, Lucas S, Murrell C, Shave R, Thomas KN, Williams MJ, Atkinson G. Elevation in cerebral blood flow velocity with aerobic fitness throughout healthy human ageing. J Physiol. 2008 Aug 15;586(16):4005-10. doi: 10.1113/jphysiol.2008.158279.

Ajam A, Aziz AA, Asirvadam VS, Muda AS, Faye I, Safdar Gardezi SJ. A review on segmentation and modeling of cerebral vasculature for surgical planning. IEEE Access. 2017;5:15222–15240.

Ajiboye N, Chalouhi N, Starke RM, Zanaty M, Bell R. Unruptured Cerebral Aneurysms: Evaluation and Management. ScientificWorldJournal. 2015;2015:954954. doi: 10.1155/2015/954954. Epub 2015 Jun 4.

Alastruey J, Parker KH, Peiró J, Byrd SM, Sherwin SJ. Modelling the circle of Willis to assess the effects of anatomical variations and occlusions on cerebral flows. J Biomech. 2007;40(8):1794-805.

Alowayyed S, Závodszky G, Azizi V, Hoekstra AG. 2018. Load Balancing of Parallel Cell-Based Blood Flow Simulations. Journal of Computational Science 24 (January): 1–7.

Alnaes MS, Isaksen J, Mardal KA, Romner B, Morgan MK, Ingebrigtsen T. Computation of hemodynamics in the circle of Willis. Stroke. 2007 Sep;38(9):2500-5. doi: 10.1161/STROKEAHA.107.482471. Epub 2007 Aug 2.

Anand S, Diamond SL. Computer simulation of systemic circulation and clot lysis dynamics during thrombolytic therapy that accounts for inner clot transport and reaction. Circulation. 1996 Aug 15;94(4):763-74. doi: 10.1161/01.cir.94.4.763.

Anor T, Grinberg L, Baek H, Madsen JR, Jayaraman MV, Karniadakis GE. Modeling of blood flow in arterial trees. Wiley Interdiscip Rev Syst Biol Med. 2010 Sep-Oct;2(5):612-623. doi: 10.1002/wsbm.90.

Aries MJ, Elting JW, De Keyser J, Kremer BP, Vroomen PC. Cerebral autoregulation in stroke: a review of transcranial Doppler studies. Stroke. 2010 Nov;41(11):2697-704.

Arvanitakis Z, Capuano AW, Leurgans SE, Bennett DA, Schneider JA. Relation of cerebral vessel disease to Alzheimer's disease dementia and cognitive function in elderly people: a cross-sectional study. Lancet Neurol. 2016 Aug;15(9):934-943. doi: 10.1016/S1474-4422(16)30029-1. Epub 2016 Jun 14.

Balogh P, Bagchi P. Direct Numerical Simulation of Cellular-Scale Blood Flow in 3D Microvascular Networks. Biophys J. 2017 Dec 19;113(12):2815-2826. doi: 10.1016/j.bpj.2017.10.020.

Bannish BE, Keener JP, Fogelson AL. Modelling fibrinolysis: a 3D stochastic multiscale model. Math Med Biol. 2014 Mar;31(1):17-44. doi: 10.1093/imammb/dqs029. Epub 2012 Dec 4.

Bárdossy G, Halász G. 2011. Modeling Blood Flow in the Arterial System. Periodica Polytechnica Mechanical Engineering 55 (1): 49–55.

Bazilevs Y, Hsu MC, Zhang Y, Wang W, Kvamsdal T, Hentschel S, Isaksen JG. Computational vascular fluid-structure interaction: methodology and application to cerebral aneurysms. Biomech Model Mechanobiol. 2010 Aug;9(4):481-98. doi: 10.1007/s10237-010-0189-7. Epub 2010 Jan 29.

Beard DA. Computational framework for generating transport models from databases of microvascular anatomy. Ann Biomed Eng. 2001 Oct;29(10):837-43. doi: 10.1114/1.1408920.

Belyaev AV, Dunster JL, Gibbins JM, Panteleev MA, Volpert V. Modeling thrombosis in silico: Frontiers, challenges, unresolved problems and milestones. Phys Life Rev. 2018 Nov;26-27:57-95. doi: 10.1016/j.plrev.2018.02.005. Epub 2018 Mar 5.

Bendich P, Marron JS, Miller E, Pieloch A, Skwerer S. Persistent Homology Analysis of Brain Artery Trees. Ann Appl Stat. 2016;10(1):198-218. doi: 10.1214/15-AOAS886. Epub 2016 Mar 25.

Beratlis N, Balaras E, Parvinian B, Kiger K. A numerical and experimental investigation of transitional pulsatile flow in a stenosed channel. J Biomech Eng. 2005 Dec;127(7):1147-57. doi: 10.1115/1.2073628.

Berg P, Stucht D, Janiga G, Beuing O, Speck O, Thévenin D. Cerebral blood flow in a healthy Circle of Willis and two intracranial aneurysms: computational fluid dynamics versus four-dimensional phase-contrast magnetic resonance imaging. J Biomech Eng. 2014 Apr;136(4). doi: 10.1115/1.4026108.

Berg P, Radtke L, Vos S, Serowy S, Janiga G, Preim B, Beuing O, Saalfeld S. 3DRA Reconstruction of Intracranial Aneurysms - How does Voxel Size Influences Morphologic and Hemodynamic Parameters. Annu Int Conf IEEE Eng Med Biol Soc. 2018 Jul;2018:1327-1330. doi: 10.1109/EMBC.2018.8512524.

Berg P, Voß S, Janiga G, Saalfeld S, Bergersen AW, Valen-Sendstad K, Bruening J, Goubergrits L, Spuler A, Chiu TL, Tsang ACO, Copelli G, Csippa B, Paál G, Závodszky G, Detmer FJ, Chung BJ, Cebral JR, Fujimura S, Takao H, Karmonik C, Elias S, Cancelliere NM, Najafi M, Steinman DA, Pereira VM, Piskin S, Finol EA, Pravdivtseva M, Velvaluri P, Rajabzadeh-Oghaz H, Paliwal N, Meng H, Seshadhri S, Venguru S, Shojima M, Sindeev S, Frolov S, Qian Y, Wu YA, Carlson KD, Kallmes DF, Dragomir-Daescu D, Beuing O. Multiple Aneurysms AnaTomy CHallenge 2018 (MATCH)-phase II: rupture risk assessment. Int J Comput Assist Radiol Surg. 2019 Oct;14(10):1795-1804. doi: 10.1007/s11548-019-01986-2. Epub 2019 May 3.

Berkhemer OA, Fransen PS, Beumer D, van den Berg LA, Lingsma HF, Yoo AJ, Schonewille WJ, Vos JA, Nederkoorn PJ, Wermer MJ, van Walderveen MA, Staals J, Hofmeijer J, van Oostayen JA, Lycklama à Nijeholt GJ, Boiten J, Brouwer PA, Emmer BJ, de Bruijn SF, van Dijk LC, Kappelle LJ, Lo RH, van Dijk EJ, de Vries J, de Kort PL, van Rooij WJ, van den Berg JS, van Hasselt BA, Aerden LA, Dallinga RJ, Visser MC, Bot JC, Vroomen PC, Eshghi O, Schreuder TH, Heijboer RJ, Keizer K, Tielbeek AV, den Hertog HM, Gerrits DG, van den Berg-Vos RM, Karas GB, Steyerberg EW, Flach HZ, Marquering HA, Sprengers ME, Jenniskens SF, Beenen LF, van den Berg R, Koudstaal PJ, van Zwam WH, Roos YB, van der Lugt A, van Oostenbrugge RJ, Majoie CB, Dippel DW; MR CLEAN Investigators. A randomized trial of intraarterial treatment for acute ischemic stroke. N Engl J Med. 2015 Jan 1;372(1):11-20. doi: 10.1056/NEJMoa1411587. Erratum in: N Engl J Med. 2015 Jan 22;372(4):394.

Bernabeu MO, Köry J, Grogan JA, Markelc B, Beardo A, d'Avezac M, Enjalbert R, Kaeppler J, Daly N, Hetherington J, Krüger T, Maini PK, Pitt-Francis JM, Muschel RJ, Alarcón T, Byrne HM. Abnormal morphology biases hematocrit distribution in tumor vasculature and contributes to heterogeneity in tissue oxygenation. Proc Natl Acad Sci U S A. 2020 Nov 10;117(45):27811-27819. doi: 10.1073/pnas.2007770117. Epub 2020 Oct 27.

Bernier M, Cunnane SC, Whittingstall K. The morphology of the human cerebrovascular system. Hum Brain Mapp. 2018 Dec;39(12):4962-4975. doi: 10.1002/hbm.24337. Epub 2018 Sep 28.

Blinder P, Tsai PS, Kaufhold JP, Knutsen PM, Suhl H, Kleinfeld D. The cortical angiome: an interconnected vascular network with noncolumnar patterns of blood flow. Nat Neurosci. 2013 Jul;16(7):889-97. doi: 10.1038/nn.3426.

Boas DA, Campbell LE, Yodh AG. Scattering and Imaging with Diffusing Temporal Field Correlations. Phys Rev Lett. 1995 Aug 28;75(9):1855-1858.

Boas DA, Jones SR, Devor A, Huppert TJ, Dale AM. A vascular anatomical network model of the spatio-temporal response to brain activation. Neuroimage. 2008 Apr 15;40(3):1116-29.

Bogunović H, Pozo JM, Villa-Uriol MC, Majoie CB, van den Berg R, Gratama van Andel HA, Macho JM, Blasco J, Román LS, Frangi AF. Automated segmentation of cerebral vasculature with aneurysms in 3DRA and TOF-MRA using geodesic active regions: an evaluation study. Med Phys. 2011 Jan;38(1):210-22. doi: 10.1118/1.3515749.

Bollmann S, Mattern H, Bernier M, Robinson SD, Park D, Speck O, Polimeni JR. Imaging of the pial arterial vasculature of the human brain in vivo using high-resolution 7T time-of-flight angiography. Elife. 2022 Apr 29;11:e71186. doi: 10.7554/eLife.71186.

Botti L, Paliwal N, Conti P, Antiga L, Meng H. Modeling hemodynamics in intracranial aneurysms: Comparing accuracy of CFD solvers based on finite element and finite volume schemes. Int J Numer Method Biomed Eng. 2018 Sep;34(9):e3111. doi: 10.1002/cnm.3111. Epub 2018 Jul 20.

Boyd J, Buick JM. Comparison of Newtonian and non-Newtonian flows in a two-dimensional carotid artery model using the lattice Boltzmann method. Phys Med Biol. 2007 Oct 21;52(20):6215-28. doi: 10.1088/0031-9155/52/20/009. Epub 2007 Oct 1.

Brinjikji W, Nogueira RG, Kvamme P, Layton KF, Delgado Almandoz JE, Hanel RA, Mendes Pereira V, Almekhlafi MA, Yoo AJ, Jahromi BS, Gounis MJ, Patel B, Abbasi M, Fitzgerald S, Mereuta OM, Dai D, Kadirvel R, Doyle K, Savastano L, Cloft HJ, Haussen DC, Al-Bayati AR, Mohammaden MH, Pisani L, Rodrigues GM, Thacker IC, Kayan Y, Copelan A, Aghaebrahim A, Sauvageau E, Demchuk AM, Bhuva P, Soomro J, Nazari P, Cantrell DR, Puri AS, Entwistle J, Polley EC, Kallmes DF. Association between clot composition and stroke origin in mechanical thrombectomy patients: analysis of the Stroke Thromboembolism Registry of Imaging and Pathology. J Neurointerv Surg. 2021 Jul;13(7):594-598. doi: 10.1136/neurintsurg-2020-017167. Epub 2021 Mar 15.

Brisman JL, Niimi Y, Song JK, Berenstein A. Aneurysmal rupture during coiling: low incidence and good outcomes at a single large volume center. Neurosurgery. 2005 Dec;57(6):1103-9; discussion 1103-9. doi: 10.1227/01.neu.0000185631.20246.1a.

Brown WR, Thore CR. Review: cerebral microvascular pathology in ageing and neurodegeneration. Neuropathol Appl Neurobiol. 2011 Feb;37(1):56-74. doi: 10.1111/j.1365-2990.2010.01139.x.

Campbell BC, Mitchell PJ, Kleinig TJ, Dewey HM, Churilov L, Yassi N, Yan B, Dowling RJ, Parsons MW, Oxley TJ, Wu TY, Brooks M, Simpson MA, Miteff F, Levi CR, Krause M, Harrington TJ,

Faulder KC, Steinfort BS, Priglinger M, Ang T, Scroop R, Barber PA, McGuinness B, Wijeratne T, Phan TG, Chong W, Chandra RV, Bladin CF, Badve M, Rice H, de Villiers L, Ma H, Desmond PM, Donnan GA, Davis SM; EXTEND-IA Investigators. Endovascular therapy for ischemic stroke with perfusion-imaging selection. N Engl J Med. 2015 Mar 12;372(11):1009-18. doi: 10.1056/NEJMoa1414792.

Carey BJ, Eames PJ, Blake MJ, Panerai RB, Potter JF. Dynamic cerebral autoregulation is unaffected by aging. Stroke. 2000 Dec;31(12):2895-900.

Caro CG, Pedley TJ, Schroter RC and Seed WA. The mechanics of the circulation (2nd edition). Cambridge University Press, 2012.

Cassot F, Lauwers F, Lorthois S, Puwanarajah P, Duvernoy H. Scaling laws for branching vessels of human cerebral cortex. Microcirculation. 2009 May;16(4):331-44, 2 p following 344. doi: 10.1080/10739680802662607.

Cebral JR, Putman CM, Alley MT, Hope T, Bammer R, Calamante F. Hemodynamics in Normal Cerebral Arteries: Qualitative Comparison of 4D Phase-Contrast Magnetic Resonance and Image-Based Computational Fluid Dynamics. J Eng Math. 2009 Aug 1;64(4):367-378. doi: 10.1007/s10665-009-9266-2.

Cebral JR, Yim PJ, Löhner R, Soto O, Choyke PL. Blood flow modeling in carotid arteries with computational fluid dynamics and MR imaging. Acad Radiol. 2002 Nov;9(11):1286-99.

Chappell MA, Payne SJ. Physiology for Engineers, 2nd edition. Springer. 2020.

Chen Y, Liu YN, Zhou P, Zhang X, Wu Q, Zhao X, Ming D. The Transitions Between Dynamic Micro-States Reveal Age-Related Functional Network Reorganization. Front Physiol. 2019 Jan 4;9:1852. doi: 10.3389/fphys.2018.01852. eCollection 2018.

Chen L, Mossa-Basha M, Sun J, Hippe DS, Balu N, Yuan Q, Pimentel K, Hatsukami TS, Hwang JN, Yuan C. Quantification of morphometry and intensity features of intracranial arteries from 3D TOF MRA using the intracranial artery feature extraction (iCafe): A reproducibility study. Magn Reson Imaging. 2019 Apr;57:293-302. doi: 10.1016/j.mri.2018.12.007. Epub 2018 Dec 20.

Chiastra C, Migliori S, Burzotta F, Dubini G, Migliavacca F. Patient-Specific Modeling of Stented Coronary Arteries Reconstructed from Optical Coherence Tomography: Towards a Widespread Clinical Use of Fluid Dynamics Analyses. J Cardiovasc Transl Res. 2018 Apr;11(2):156-172. doi: 10.1007/s12265-017-9777-6. Epub 2017 Dec 27.

Chopard B, de Sousa DR, Lätt J, Mountrakis L, Dubois F, Yourassowsky C, Van Antwerpen P, Eker O, Vanhamme L, Perez-Morga D, Courbebaisse G, Lorenz E, Hoekstra AG, Boudjeltia KZ. A physical description of the adhesion and aggregation of platelets. R Soc Open Sci. 2017 Apr 12;4(4):170219. doi: 10.1098/rsos.170219. eCollection 2017 Apr.

Chou D, Vardakis JC, Guo L, Tully BJ, Ventikos Y. A fully dynamic multi-compartmental poroelastic system: Application to aqueductal stenosis. J Biomech. 2016 Jul 26;49(11):2306-2312. doi: 10.1016/j.jbiomech.2015.11.025. Epub 2015 Nov 28.

Chueh JY, Puri AS, Gounis MJ. An in vitro evaluation of distal emboli following Lazarus Cover-assisted stent retriever thrombectomy. J Neurointerv Surg. 2017 Feb;9(2):183-187. doi: 10.1136/neurintsurg-2015-012256. Epub 2016 Feb 26.

Chueh JY, Marosfoi MG, Anagnostakou V, Arslanian RA, Marks MP, Gounis MJ. Quantitative Characterization of Recanalization and Distal Emboli with a Novel Thrombectomy Device. Cardiovasc Intervent Radiol. 2021 Feb;44(2):318-324. doi: 10.1007/s00270-020-02683-3. Epub 2020 Nov 11.

Connolly ES Jr, Solomon RA. Management of symptomatic and asymptomatic unruptured aneurysms. Neurosurg Clin N Am. 1998 Jul;9(3):509-24.

Cool, D. et al. Tissue-Based Affine Registration of Brain Images to form a Vascular Density Atlas. Medical Image Computing and Computer-Assisted Intervention, 9–15 (2003).

Correia M, Provost J, Tanter M, Pernot M. 4D ultrafast ultrasound flow imaging: in vivo quantification of arterial volumetric flow rate in a single heartbeat. Phys Med Biol. 2016 Dec 7;61(23):L48-L61.

Czaja B, de Bouter J, Heisler M, Závodszky G, Karst S, Sarunic M, Maberley D, Hoekstra A. The effect of stiffened diabetic red blood cells on wall shear stress in a reconstructed 3D microaneurysm.Comput Methods Biomech Biomed Engin. 2022 Nov;25(15):1691-1709. doi: 10.1080/10255842.2022.2034794. Epub 2022 Feb 24.

Czosnyka M, Miller C; Participants in the International Multidisciplinary Consensus Conference on Multimodality Monitoring. Monitoring of cerebral autoregulation. Neurocrit Care. 2014 Dec;21 Suppl 2:S95-102. doi: 10.1007/s12028-014-0046-0. Review.

de la Torre J. The Vascular Hypothesis of Alzheimer's Disease: A Key to Preclinical Prediction of Dementia Using Neuroimaging. J Alzheimers Dis. 2018;63(1):35-52. doi: 10.3233/JAD-180004.

den Abeelen AS, Lagro J, van Beek AH, Claassen JA. Impaired cerebral autoregulation and vasomotor reactivity in sporadic Alzheimer's disease. Curr Alzheimer Res. 2014 Jan;11(1):11-7.

Deshpande A, Jamilpour N, Jiang B, Michel P, Eskandari A, Kidwell C, Wintermark M, Laksari K. Automatic segmentation, feature extraction and comparison of healthy and stroke cerebral vasculature. Neuroimage Clin. 2021;30:102573. doi: 10.1016/j.nicl.2021.102573. Epub 2021 Jan 26.

Dufour A, Tankyevych O, Talbot H, Ronse C. A statistical arteriovenous cerebral atlas. MICCAI Workshop on Computing and Visualization for (Intra)Vascular Imaging, 73–80 (2011).

Dunås T, Wåhlin A, Ambarki K, Zarrinkoob L, Malm J, Eklund A. A Stereotactic Probabilistic Atlas for the Major Cerebral Arteries. Neuroinformatics. 2017 Jan;15(1):101-110. doi: 10.1007/s12021-016-9320-y.

Dutta S, Sengupta P. Men and mice: Relating their ages. Life Sci. 2016 May 1;152:244-8. doi: 10.1016/j.lfs.2015.10.025. Epub 2015 Oct 24.

Duvernoy HM, Delon S, Vannson JL. Cortical blood vessels of the human brain. Brain Res Bull. 1981 Nov;7(5):519-79.

Ebrahimi S, Bagchi P. A computational study of red blood cell deformability effect on hemodynamic alteration in capillary vessel networks. Sci Rep. 2022 Mar 11;12(1):4304. doi: 10.1038/s41598-022-08357-z.

El-Bouri WK, Payne SJ. Multi-scale homogenization of blood flow in 3-dimensional human cerebral microvascular networks. J Theor Biol. 2015 Sep 7;380:40-7.

El-Bouri WK, Payne SJ. A statistical model of the penetrating arterioles and venules in the human cerebral cortex. Microcirculation. 2016 Oct;23(7):580-590. doi: 10.1111/micc.12318.

El-Bouri WK, MacGowan A, Józsa TI, Gounis MJ, Payne SJ. Modelling the impact of clot fragmentation on the microcirculation after thrombectomy. PLoS Comput Biol. 2021 Mar 12;17(3):e1008515. doi: 10.1371/journal.pcbi.1008515. eCollection 2021 Mar.

Enjalbert R, Hardman D, Krüger T, Bernabeu MO. Compressed vessels bias red blood cell partitioning at bifurcations in a hematocrit-dependent manner: Implications in tumor blood flow. Proc Natl Acad Sci U S A. 2021 Jun 22;118(25):e2025236118. doi: 10.1073/pnas.2025236118. Epub 2021 Jun 17.

Ertürk A, Becker K, Jährling N, Mauch CP, Hojer CD, Egen JG, Hellal F, Bradke F, Sheng M, Dodt HU. Three-dimensional imaging of solvent-cleared organs using 3DISCO. Nat Protoc. 2012 Nov;7(11):1983-95. doi: 10.1038/nprot.2012.119. Epub 2012 Oct 11.

Fang Q, Sakadzic S, Ruvinskaya L, Devor A, Dale AM, Boas DA. Oxygen advection and diffusion in a three- dimensional vascular anatomical network. Optics Express. 2008;16:17530–17541.

Farkas E, Süle Z, Tóth-Szuki V, Mátyás A, Antal P, Farkas IG, Mihály A, Bari F. Tumor necrosis factor-alpha increases cerebral blood flow and ultrastructural capillary damage through the release of nitric oxide in the rat brain. Microvasc Res. 2006 Nov;72(3):113-9. doi: 10.1016/j.mvr.2006.05.007. Epub 2006 Jul 18.

Fedosov DA, Lei H, Caswell B, Suresh S, Karniadakis GE. Multiscale modeling of red blood cell mechanics and blood flow in malaria. PLoS Comput Biol. 2011 Dec;7(12):e1002270. doi: 10.1371/journal.pcbi.1002270. Epub 2011 Dec 1.

Fereidoonnezhad B, Moerman KM, Johnson S, McCarthy R, McGarry PJ. A new compressible hyperelastic model for the multi-axial deformation of blood clot occlusions in vessels.

Biomech Model Mechanobiol. 2021 Aug;20(4):1317-1335. doi: 10.1007/s10237-021-01446-4. Epub 2021 Apr 5.

Fereidoonnezhad B, McGarry P. A new constitutive model for permanent deformation of blood clots with application to simulation of aspiration thrombectomy. J Biomech. 2022 Jan;130:110865. doi: 10.1016/j.jbiomech.2021.110865. Epub 2021 Nov 12.

Fogelson AL, Neeves KB. Fluid Mechanics of Blood Clot Formation. Annu Rev Fluid Mech. 2015 Jan 1;47:377-403. doi: 10.1146/annurev-fluid-010814-014513.

Flasque N, Desvignes M, Constans JM, Revenu M. Acquisition, segmentation and tracking of the cerebral vascular tree on 3D magnetic resonance angiography images. Med Image Anal. 2001 Sep;5(3):173-83. doi: 10.1016/s1361-8415(01)00038-x.

Flores J, Alastruey J, Corvera Poiré E. A Novel Analytical Approach to Pulsatile Blood Flow in the Arterial Network. Ann Biomed Eng. 2016 May 2.

Flurkey K, Brandvain Y, Klebanov S, Austad SN, Miller RA, Yuan R, Harrison DE. PohnB6F1: a cross of wild and domestic mice that is a new model of extended female reproductive life span. J Gerontol A Biol Sci Med Sci. 2007 Nov;62(11):1187-98. doi: 10.1093/gerona/62.11.1187.

Fung YC, Tsang WC, Patitucci P. High-resolution data on the geometry of red blood cells. Biorheology. 1981;18(3-6):369-85. doi: 10.3233/bir-1981-183-606.

Gagnon L, Sakadžić S, Lesage F, Musacchia JJ, Lefebvre J, Fang Q, Yücel MA, Evans KC, Mandeville ET, Cohen-Adad J, Polimeni JR, Yaseen MA, Lo EH, Greve DN, Buxton RB, Dale AM, Devor A, Boas DA. Quantifying the microvascular origin of BOLD-fMRI from first principles with two-photon microscopy and an oxygen-sensitive nanoprobe. J Neurosci. 2015 Feb 25;35(8):3663-75. doi: 10.1523/JNEUROSCI.3555-14.2015.

Gagnon L, Smith AF, Boas DA, Devor A, Secomb TW, Sakadžić S. Modeling of Cerebral Oxygen Transport Based on In vivo Microscopic Imaging of Microvascular Network Structure, Blood Flow, and Oxygenation. Front Comput Neurosci. 2016; 10: 82. Published online 2016 Aug 31.

Gao LY, Guo X, Zhou JJ, Zhang Q, Fu J, Chen WJ, Yang YJ. Basilar artery fenestration detected with CT angiography. Eur Radiol. 2013 Oct;23(10):2861-7. doi: 10.1007/s00330-013-2890-2. Epub 2013 May 23.

Gkontra P, El-Bouri WK, Norton KA, Santos A, Popel AS, Payne SJ, Arroyo AG. Dynamic Changes in Microvascular Flow Conductivity and Perfusion After Myocardial Infarction Shown by Image-Based Modeling. J Am Heart Assoc. 2019 Apr 2;8(7):e011058. doi: 10.1161/JAHA.118.011058.

Goirand F, Le Borgne T, Lorthois S. Network-driven anomalous transport is a fundamental component of brain microvascular dysfunction. Nat Commun. 2021 Dec 15;12(1):7295. doi: 10.1038/s41467-021-27534-8.

Goswami P, Markey MK, Warach SJ, Dula AN. Quantitative Analysis of the Cerebral Vasculature on Magnetic Resonance Angiography. Sci Rep. 2020 Jun 23;10(1):10227. doi: 10.1038/s41598-020-67225-w.

Goubergrits L, Schaller J, Kertzscher U, Woelken T, Ringelstein M, Spuler A. Hemodynamic impact of cerebral aneurysm endovascular treatment devices: coils and flow diverters. Expert Rev Med Devices. 2014 Jul;11(4):361-73. doi: 10.1586/17434440.2014.925395.

Gould IG, Linninger AA. Hematocrit distribution and tissue oxygenation in large microcirculatory networks. Microcirculation. 2015 Jan;22(1):1-18. doi: 10.1111/micc.12156.

Gould IG, Tsai P, Kleinfeld D, Linninger A. The capillary bed offers the largest hemodynamic resistance to the cortical blood supply. J Cereb Blood Flow Metab. 2017 Jan;37(1):52-68.

Goyal M, Menon BK, van Zwam WH, Dippel DW, Mitchell PJ, Demchuk AM, Dávalos A, Majoie CB, van der Lugt A, de Miquel MA, Donnan GA, Roos YB, Bonafe A, Jahan R, Diener HC, van den Berg LA, Levy EI, Berkhemer OA, Pereira VM, Rempel J, Millán M, Davis SM, Roy D, Thornton J, Román LS, Ribó M, Beumer D, Stouch B, Brown S, Campbell BC, van Oostenbrugge RJ, Saver JL, Hill MD, Jovin TG; HERMES collaborators. Endovascular thrombectomy after large-vessel ischaemic stroke: a meta-analysis of individual patient data from five randomised trials. Lancet. 2016 Apr 23;387(10029):1723-31. doi: 10.1016/S0140-6736(16)00163-X.

Graff BJ, Payne SJ, El-Bouri WK. The Ageing Brain: Investigating the Role of Age in Changes to the Human Cerebral Microvasculature With an in silico Model. Front Aging Neurosci. 2021 Aug 5;13:632521. doi: 10.3389/fnagi.2021.632521. eCollection 2021.

Graff BJ, Harrison SL, Payne SJ, El-Bouri WK. Regional Cerebral Blood Flow Changes in Healthy Ageing and Alzheimer's Disease: A Narrative Review. Cerebrovasc Dis. 2022 May 31:1-10. doi: 10.1159/000524797. Online ahead of print.

Gu B, Piebalgs A, Huang Y, Roi D, Lobotesis K, Longstaff C, Hughes AD, Chen R, Thom SA, Xu XY. Computational simulations of thrombolysis in acute stroke: Effect of clot size and location on recanalisation. Med Eng Phys. 2019 Nov;73:9-17. doi: 10.1016/j.medengphy.2019.07.014. Epub 2019 Aug 8.

Gu B, Huang Y, Manchester EL, Hughes AD, Thom SAM, Chen R, Xu XY. Multiphysics Modelling and Simulation of Thrombolysis via Activated Platelet-Targeted Nanomedicine. Pharm Res. 2022 Jan;39(1):41-56. doi: 10.1007/s11095-021-03161-2. Epub 2022 Jan 19.

Guibert R, Fonta C, Plourabouré F. Cerebral blood flow modeling in primate cortex. J Cereb Blood Flow Metab. 2010 Nov;30(11):1860-73. doi: 10.1038/jcbfm.2010.105.

Guo L, Vardakis JC, Lassila T, Mitolo M, Ravikumar N, Chou D, Lange M, Sarrami-Foroushani A, Tully BJ, Taylor ZA, Varma S, Venneri A, Frangi AF, Ventikos Y. Subject-specific multi-poroelastic model for exploring the risk factors associated with the early stages of Alzheimer's

disease. Interface Focus. 2018 Feb 6;8(1):20170019. doi: 10.1098/rsfs.2017.0019. Epub 2017 Dec 15.

Gutierrez J, Cheung K, Bagci A, Rundek T, Alperin N, Sacco RL, Wright CB, Elkind MS. Brain Arterial Diameters as a Risk Factor for Vascular Events. J Am Heart Assoc. 2015 Aug 6;4(8):e002289. doi: 10.1161/JAHA.115.002289.

Gutierrez J, Honig L, Elkind MS, Mohr JP, Goldman J, Dwork AJ, Morgello S, Marshall RS. Brain arterial aging and its relationship to Alzheimer dementia. Neurology. 2016 Apr 19;86(16):1507-15. doi: 10.1212/WNL.0000000000002590. Epub 2016 Mar 16.

Hall CN, Reynell C, Gesslein B, Hamilton NB, Mishra A, Sutherland BA, O'Farrell FM, Buchan AM, Lauritzen M, Attwell D. Capillary pericytes regulate cerebral blood flow in health and disease. Nature. 2014 Apr 3;508(7494):55-60. doi: 10.1038/nature13165.

Hartmann DA, Coelho-Santos V, Shih AY. Pericyte Control of Blood Flow Across Microvascular Zones in the Central Nervous System. Annu Rev Physiol. 2022 Feb 10;84:331-354. doi: 10.1146/annurev-physiol-061121-040127. Epub 2021 Oct 21.

Hartung G, Vesel C, Morley R, Alaraj A, Sled J, Kleinfeld D, Linninger A. Simulations of blood as a suspension predicts a depth dependent hematocrit in the circulation throughout the cerebral cortex. PLoS Comput Biol. 2018 Nov 19;14(11):e1006549. doi: 10.1371/journal.pcbi.1006549. eCollection 2018 Nov.

Hartung G, Badr S, Mihelic S, Dunn A, Cheng X, Kura S, Boas DA, Kleinfeld D, Alaraj A, Linninger AA. Mathematical synthesis of the cortical circulation for the whole mouse brain-part II: Microcirculatory closure. Microcirculation. 2021 Jul;28(5):e12687. doi: 10.1111/micc.12687. Epub 2021 Apr 8.

Hashemi Z, Rahnama M. Numerical simulation of transient dynamic behavior of healthy and hardened red blood cells in microcapillary flow. Int J Numer Method Biomed Eng. 2016 Nov;32(11). doi: 10.1002/cnm.2763. Epub 2016 Jan 20.

Hedman AM, van Haren NE, Schnack HG, Kahn RS, Hulshoff Pol HE. Human brain changes across the life span: a review of 56 longitudinal magnetic resonance imaging studies. Hum Brain Mapp. 2012 Aug;33(8):1987-2002. doi: 10.1002/hbm.21334. Epub 2011 Sep 13.

Higashida RT, Furlan AJ, Roberts H, Tomsick T, Connors B, Barr J, Dillon W, Warach S, Broderick J, Tilley B, Sacks D; Technology Assessment Committee of the American Society of Interventional and Therapeutic Neuroradiology; Technology Assessment Committee of the Society of Interventional Radiology. Trial design and reporting standards for intra-arterial cerebral thrombolysis for acute ischemic stroke. Stroke. 2003 Aug;34(8):e109-37.

Hindenes LB, Håberg AK, Johnsen LH, Mathiesen EB, Robben D, Vangberg TR. Variations in the Circle of Willis in a large population sample using 3D TOF angiography: The Tromsø Study. PLoS One. 2020 Nov 3;15(11):e0241373. doi: 10.1371/journal.pone.0241373. eCollection 2020.

Ho H, Mithraratne K, Schmid H, Sands G, Hunter P. Computer simulation of vertebral artery occlusion in endovascular procedures. Int J Comput Assist Radiol Surg. 2010 Jan;5(1):29-37. doi: 10.1007/s11548-009-0379-x. Epub 2009 Jun 23.

Horton NG, Wang K, Kobat D, Clark CG, Wise FW, Schaffer CB, Xu C. In vivo three-photon microscopy of subcortical structures within an intact mouse brain. Nat Photonics. 2013 Mar 1;7(3):205-9. doi: 10.1038/nphoton.2012.336.

Hsu CY, Ghaffari M, Alaraj A, Flannery M, Zhou XJ, Linninger A. Gap-free segmentation of vascular networks with automatic image processing pipeline. Comput Biol Med. 2017 Mar 1;82:29-39. doi: 10.1016/j.compbiomed.2017.01.012. Epub 2017 Jan 21.

Huang C, Shi B, Guo Z, Chai Z. 2015. Multi-GPU Based Lattice Boltzmann Method for Hemodynamic Simulation in Patient-Specific Cerebral Aneurysm. Communications in Computational Physics 17 (4): 960–74.

Huo Y, Kassab GS. Intraspecific scaling laws of vascular trees. J R Soc Interface. 2012 Jan 7;9(66):190-200. doi: 10.1098/rsif.2011.0270.

Ihn YK, Shin SH, Baik SK, Choi IS. Complications of endovascular treatment for intracranial aneurysms: Management and prevention. Interv Neuroradiol. 2018 Jun;24(3):237-245. doi: 10.1177/1591019918758493. Epub 2018 Feb 21.

Iliff JJ, Wang M, Zeppenfeld DM, Venkataraman A, Plog BA, Liao Y, Deane R, Nedergaard M. Cerebral arterial pulsation drives paravascular CSF-interstitial fluid exchange in the murine brain. J Neurosci. 2013 Nov 13;33(46):18190-9. doi: 10.1523/JNEUROSCI.1592-13.2013.

Ishida F, Tsuji M, Tanioka S, Tanaka K, Yoshimura S, Suzuki H. Computational Fluid Dynamics for Cerebral Aneurysms in Clinical Settings. Acta Neurochir Suppl. 2021;132:27-32. doi: 10.1007/978-3-030-63453-7_4.

Janiga G, Daróczy L, Berg P, Thévenin D, Skalej M, Beuing O. An automatic CFD-based flow diverter optimization principle for patient-specific intracranial aneurysms. J Biomech. 2015 Nov 5;48(14):3846-52. doi: 10.1016/j.jbiomech.2015.09.039. Epub 2015 Oct 3.

Jansen IG, Schneiders JJ, Potters WV, van Ooij P, van den Berg R, van Bavel E, Marquering HA, Majoie CB. Generalized versus patient-specific inflow boundary conditions in computational fluid dynamics simulations of cerebral aneurysmal hemodynamics. AJNR Am J Neuroradiol. 2014 Aug;35(8):1543-8. doi: 10.3174/ajnr.A3901. Epub 2014 Mar 20.

Jeong W, Rhee K. Hemodynamics of cerebral aneurysms: computational analyses of aneurysm progress and treatment. Comput Math Methods Med. 2012;2012:782801. doi: 10.1155/2012/782801. Epub 2012 Feb 19.

Jespersen SN, Østergaard L. The roles of cerebral blood flow, capillary transit time heterogeneity, and oxygen tension in brain oxygenation and metabolism. J Cereb Blood Flow Metab. 2012 Feb;32(2):264-77. doi: 10.1038/jcbfm.2011.153.

Jöbsis FF. Noninvasive, infrared monitoring of cerebral and myocardial oxygen sufficiency and circulatory parameters. Science. 1977 Dec 23;198(4323):1264-7.

Johnson S, Duffy S, Gunning G, Gilvarry M, McGarry JP, McHugh PE. Review of Mechanical Testing and Modelling of Thrombus Material for Vascular Implant and Device Design. Ann Biomed Eng. 2017 Nov;45(11):2494-2508. doi: 10.1007/s10439-017-1906-5. Epub 2017 Aug 28.

Johnson S, McCarthy R, Gilvarry M, McHugh PE, McGarry JP. Investigating the Mechanical Behavior of Clot Analogues Through Experimental and Computational Analysis. Ann Biomed Eng. 2021 Jan;49(1):420-431. doi: 10.1007/s10439-020-02570-5. Epub 2020 Jul 20.

Józsa TI, Padmos RM, Samuels N, El-Bouri WK, Hoekstra AG, Payne SJ. A porous circulation model of the human brain for in silico clinical trials in ischaemic stroke. Interface Focus. 2021 Feb 6;11(1):20190127. doi: 10.1098/rsfs.2019.0127. Epub 2020 Dec 11.

Ju M, Ye SS, Namgung B, Cho S, Low HT, Leo HL, Kim S. A review of numerical methods for red blood cell flow simulation. Comput Methods Biomech Biomed Engin. 2015;18(2):130-40. doi: 10.1080/10255842.2013.783574.

Kamenskiy AV, Pipinos II, Carson JS, MacTaggart JN, Baxter BT. Age and disease-related geometric and structural remodeling of the carotid artery. J Vasc Surg. 2015 Dec;62(6):1521-8. doi: 10.1016/j.jvs.2014.10.041. Epub 2014 Dec 9.

Kety SS, Schmidt CF. The nitrous oxide method for the quantitative determination of cerebral blood flow in man: theory, procedure and normal values. J Clin Invest. 1948 Jul;27(4):476-83.

Kim BJ, Kim SM, Kang DW, Kwon SU, Suh DC, Kim JS. Vascular tortuosity may be related to intracranial artery atherosclerosis. Int J Stroke. 2015 Oct;10(7):1081-6. doi: 10.1111/ijs.12525. Epub 2015 Jun 9.

Kim DJ, Kasprowicz M, Carrera E, Castellani G, Zweifel C, Lavinio A, Smielewski P, Sutcliffe MP, Pickard JD, Czosnyka M. The monitoring of relative changes in compartmental compliances of brain. Physiol Meas. 2009 Jul;30(7):647-59. Doi: 10.1088/0967-3334/30/7/009. Epub 2009 Jun 5.

Kim YH, Xu X, Lee JS. The effect of stent porosity and strut shape on saccular aneurysm and its numerical analysis with lattice Boltzmann method. Ann Biomed Eng. 2010 Jul;38(7):2274-92. doi: 10.1007/s10439-010-9994-5. Epub 2010 Mar 19.

Kimura T, Morita A, Nishimura K, Aiyama H, Itoh H, Fukaya S, Sora S, Ochiai C. Simulation of and training for cerebral aneurysm clipping with 3-dimensional models. Neurosurgery. 2009 Oct;65(4):719-25; discussion 725-6. doi: 10.1227/01.NEU.0000354350.88899.07.

Kleine JF, Wunderlich S, Zimmer C, Kaesmacher J. Time to redefine success? TICI 3 versus TICI 2b recanalization in middle cerebral artery occlusion treated with thrombectomy. J

Neurointerv Surg. 2016 Feb 17. pii: neurintsurg-2015-012218. doi: 10.1136/neurintsurg-2015-012218.

Konduri PR, Marquering HA, van Bavel EE, Hoekstra A, Majoie CBLM; INSIST Investigators. In-Silico Trials for Treatment of Acute Ischemic Stroke. Front Neurol. 2020 Sep 16;11:558125. doi: 10.3389/fneur.2020.558125. eCollection 2020.

Kotsalos C, Latt J, Beny J, Chopard B. Digital blood in massively parallel CPU/GPU systems for the study of platelet transport. Interface Focus. 2021 Feb 6;11(1):20190116. doi: 10.1098/rsfs.2019.0116. Epub 2020 Dec 11.

Kühn AL, Vardar Z, Kraitem A, King RM, Anagnostakou V, Puri AS, Gounis MJ. Biomechanics and hemodynamics of stent-retrievers.J Cereb Blood Flow Metab. 2020 Dec;40(12):2350-2365. doi: 10.1177/0271678X20916002. Epub 2020 May 19.

Kulcsár Z, Ugron A, Marosfoi M, Berentei Z, Paál G, Szikora I. Hemodynamics of cerebral aneurysm initiation: the role of wall shear stress and spatial wall shear stress gradient. AJNR Am J Neuroradiol. 2011 Mar;32(3):587-94. doi: 10.3174/ajnr.A2339. Epub 2011 Feb 10.

Larrabide I, Villa-Uriol MC, Cárdenes R, Barbarito V, Carotenuto L, Geers AJ, Morales HG, Pozo JM, Mazzeo MD, Bogunović H, Omedas P, Riccobene C, Macho JM, Frangi AF. AngioLab--a software tool for morphological analysis and endovascular treatment planning of intracranial aneurysms. Comput Methods Programs Biomed. 2012 Nov;108(2):806-19. doi: 10.1016/j.cmpb.2012.05.006. Epub 2012 Jun 28.

Latt J, Coreixas C, Beny J. Cross-platform programming model for many-core lattice Boltzmann simulations. PLoS One. 2021 Apr 29;16(4):e0250306. doi: 10.1371/journal.pone.0250306. eCollection 2021.

Lauwers F, Cassot F, Lauwers-Cances V, Puwanarajah P, Duvernoy H. Morphometry of the human cerebral cortex microcirculation: general characteristics and space-related profiles. Neuroimage. 2008 Feb 1;39(3):936-48.

Leahy C, Radhakrishnan H, Weiner G, Goldberg JL, Srinivasan VJ. Mapping the 3D Connectivity of the Rat Inner Retinal Vascular Network Using OCT Angiography. Invest Ophthalmol Vis Sci. 2015 Sep;56(10):5785-93. doi: 10.1167/iovs.15-17210.

Lemasson B, Pannetier N, Coquery N, Boisserand LSB, Collomb N, Schuff N, Moseley M, Zaharchuk G, Barbier EL, Christen T. MR Vascular Fingerprinting in Stroke and Brain Tumors Models. Sci Rep. 2016 Nov 24;6:37071. doi: 10.1038/srep37071.

Lesage D, Angelini ED, Bloch I, Funka-Lea G. A review of 3D vessel lumen segmentation techniques: models, features and extraction schemes. Med Image Anal. 2009 Dec;13(6):819-45. doi: 10.1016/j.media.2009.07.011. Epub 2009 Aug 12.

Li J, Dao M, Lim CT, Suresh S. Spectrin-level modeling of the cytoskeleton and optical tweezers stretching of the erythrocyte. Biophys J. 2005 May;88(5):3707-19. doi: 10.1529/biophysj.104.047332. Epub 2005 Mar 4.

Li M, Liu L, Xi N, Wang Y, Dong Z, Xiao X, Zhang W. Atomic force microscopy imaging and mechanical properties measurement of red blood cells and aggressive cancer cells. Sci China Life Sci. 2012 Nov;55(11):968-73. doi: 10.1007/s11427-012-4399-3. Epub 2012 Nov 20.

Linninger AA, Gould IG, Marinnan T, Hsu CY, Chojecki M, Alaraj A. Cerebral microcirculation and oxygen tension in the human secondary cortex. Ann Biomed Eng. 2013 Nov;41(11):2264-84. doi: 10.1007/s10439-013-0828-0. Epub 2013 Jul 11.

Linninger A, Hartung G, Badr S, Morley R. Mathematical synthesis of the cortical circulation for the whole mouse brain-part I. theory and image integration. Comput Biol Med. 2019 Jul;110:265-275. doi: 10.1016/j.compbiomed.2019.05.004. Epub 2019 May 14.

Liu J, Wang Y, Akamatsu Y, Lee CC, Stetler RA, Lawton MT, Yang GY. Vascular remodeling after ischemic stroke: mechanisms and therapeutic potentials. Prog Neurobiol. 2014 Apr;115:138-56. doi: 10.1016/j.pneurobio.2013.11.004. Epub 2013 Nov 27.

Livne M, Rieger J, Aydin OU, Taha AA, Akay EM, Kossen T, Sobesky J, Kelleher JD, Hildebrand K, Frey D, Madai VI. A U-Net Deep Learning Framework for High Performance Vessel Segmentation in Patients With Cerebrovascular Disease. Front Neurosci. 2019 Feb 28;13:97. doi: 10.3389/fnins.2019.00097. eCollection 2019.

Lorthois S, Cassot F, Lauwers F. Simulation study of brain blood flow regulation by intra-cortical arterioles in an anatomically accurate large human vascular network: Part I: methodology and baseline flow. Neuroimage. 2011 Jan 15;54(2):1031-42.

Luo S, Zhong Y. Extraction of brain vessels from magnetic resonance angiographic images: concise literature review, challenges, and proposals. Conf Proc IEEE Eng Med Biol Soc. 2005;2005:1422-5. doi: 10.1109/IEMBS.2005.1616697.

Luraghi G, Cahalane RME, van de Ven E, Overschie SCM, Gijsen FJH, Akyildiz AC. In vitro and in silico modeling of endovascular stroke treatments for acute ischemic stroke. J Biomech. 2021 Oct 11;127:110693. doi: 10.1016/j.jbiomech.2021.110693. Epub 2021 Aug 14.

Luraghi G, Bridio S, Rodriguez Matas JF, Dubini G, Boodt N, Gijsen FJH, van der Lugt A, Fereidoonnezhad B, Moerman KM, McGarry P, Konduri PR, Arrarte Terreros N, Marquering HA, Majoie CBLM, Migliavacca F; INSIST investigators. The first virtual patient-specific thrombectomy procedure. J Biomech. 2021 Sep 20;126:110622. doi: 10.1016/j.jbiomech.2021.110622. Epub 2021 Jul 10.

MacMeccan RM, Clausen JR, Neitzel GP, Aidun CK. 2009. Simulating Deformable Particle Suspensions Using a Coupled Lattice-Boltzmann and Finite-Element Method. Journal of Fluid Mechanics 618 (January): 13–39.

Madjidyar J, Pineda Vidal L, Larsen N, Jansen O. Influence of Thrombus Composition on Thrombectomy: ADAPT vs. Balloon Guide Catheter and Stent Retriever in a Flow Model. Rofo. 2020 Mar;192(3):257-263. doi: 10.1055/a-0998-4246. Epub 2019 Sep 12.

Manchester EL, Roi D, Gu B, Xu XY, Lobotesis K. Modelling Combined Intravenous Thrombolysis and Mechanical Thrombectomy in Acute Ischaemic Stroke: Understanding the Relationship between Stent Retriever Configuration and Clot Lysis Mechanisms. Life (Basel). 2021 Nov 20;11(11):1271. doi: 10.3390/life11111271.

Marchand PJ, Lu X, Zhang C, Lesage F. Validation of red blood cell flux and velocity estimations based on optical coherence tomography intensity fluctuations. Sci Rep. 2020 Nov 11;10(1):19584. doi: 10.1038/s41598-020-76774-z.

Marshall I, Zhao S, Papathanasopoulou P, Hoskins P, Xu Y. 2004. MRI and CFD Studies of Pulsatile Flow in Healthy and Stenosed Carotid Bifurcation Models. Journal of Biomechanics 37 (5): 679–87.

Mazzeo S, Coveney PV. 2008. HemeLB: A High Performance Parallel Lattice-Boltzmann Code for Large Scale Fluid Flow in Complex Geometries. Computer Physics Communications 178 (12): 894–914.

Mehrabadi M, Casa LDC, Aidun CK, Ku DN. A Predictive Model of High Shear Thrombus Growth. Ann Biomed Eng. 2016 Aug;44(8):2339-2350. doi: 10.1007/s10439-016-1550-5. Epub 2016 Jan 21.

Meijs M, Patel A, van de Leemput SC, Prokop M, van Dijk EJ, de Leeuw FE, Meijer FJA, van Ginneken B, Manniesing R. Robust Segmentation of the Full Cerebral Vasculature in 4D CT of Suspected Stroke Patients. Sci Rep. 2017 Nov 15;7(1):15622. doi: 10.1038/s41598-017-15617-w.

Miller C, Padmos RM, van der Kolk M, Józsa TI, Samuels N, Xue Y, Payne SJ, Hoekstra AG. In silico trials for treatment of acute ischemic stroke: Design and implementation. Comput Biol Med. 2021 Oct;137:104802. doi: 10.1016/j.compbiomed.2021.104802. Epub 2021 Aug 26.

Moeini M, Lu X, Avti PK, Damseh R, Bélanger S, Picard F, Boas D, Kakkar A, Lesage F. Compromised microvascular oxygen delivery increases brain tissue vulnerability with age. Sci Rep. 2018 May 29;8(1):8219. doi: 10.1038/s41598-018-26543-w.

Mokhtarudin MJM, Payne SJ. The study of the function of AQP4 in cerebral ischaemia-reperfusion injury using poroelastic theory. Int J Numer Method Biomed Eng. 2017 Jan;33(1). doi: 10.1002/cnm.2784. Epub 2016 Apr 22.

Mokhtarudin MJ, Naim WA, Shabudin A, Payne SJ. Multiscale modelling of brain tissue oxygen and glucose dynamics in tortuous capillary during ischaemia-reperfusion. Applied Mathematical Modelling, 2022, 109, pp. 358–373.

Mokin M, Waqas M, Chin F, Rai H, Senko J, Sparks A, Ducharme RW, Springer M, Borlongan CV, Levy EI, Ionita C, Siddiqui AH. Semi-automated measurement of vascular tortuosity and

its implications for mechanical thrombectomy performance. Neuroradiology. 2021 Mar;63(3):381-389. doi: 10.1007/s00234-020-02525-6. Epub 2020 Aug 20.

Molyneux AJ, Kerr RS, Yu LM, Clarke M, Sneade M, Yarnold JA, Sandercock P; International Subarachnoid Aneurysm Trial (ISAT) Collaborative Group. International subarachnoid aneurysm trial (ISAT) of neurosurgical clipping versus endovascular coiling in 2143 patients with ruptured intracranial aneurysms: a randomised comparison of effects on survival, dependency, seizures, rebleeding, subgroups, and aneurysm occlusion. Lancet. 2005 Sep 3-9;366(9488):809-17. doi: 10.1016/S0140-6736(05)67214-5.

Moroz T, Banaji M, Tisdall M, Cooper CE, Elwell CE, Tachtsidis I. Development of a model to aid NIRS data interpretation: results from a hypercapnia study in healthy adults. Adv Exp Med Biol. 2012;737:293-300. doi: 10.1007/978-1-4614-1566-4_43.

Mouches P, Forkert ND. A statistical atlas of cerebral arteries generated using multi-center MRA datasets from healthy subjects. Sci Data. 2019 Apr 11;6(1):29. doi: 10.1038/s41597-019-0034-5.

Mousavi J S SM, Faghihi D, Sommer K, Bhurwani MMS, Patel TR, Santo B, Waqas M, Ionita C, Levy EI, Siddiqui AH, Tutino VM. Realistic computer modelling of stent retriever thrombectomy: a hybrid finite-element analysis-smoothed particle hydrodynamics model. J R Soc Interface. 2021 Dec;18(185):20210583. doi: 10.1098/rsif.2021.0583. Epub 2021 Dec 15.

Mulugeta L, Drach A, Erdemir A, Hunt CA, Horner M, Ku JP, Myers JG Jr, Vadigepalli R, Lytton WW. Credibility, Replicability, and Reproducibility in Simulation for Biomedicine and Clinical Applications in Neuroscience. Front Neuroinform. 2018 Apr 16;12:18. doi: 10.3389/fninf.2018.00018. eCollection 2018.

Murayama Y, Fujimura S, Suzuki T, Takao H. Computational fluid dynamics as a risk assessment tool for aneurysm rupture. Neurosurg Focus. 2019 Jul 1;47(1):E12. doi: 10.3171/2019.4.FOCUS19189.

Murray CD. The Physiological Principle of Minimum Work: I. The Vascular System and the Cost of Blood Volume. Proc Natl Acad Sci U S A. 1926 Mar;12(3):207-14.

Mut F, Scrivano E, Bleise C, Lylyk P, Cebral J. Hemodynamics in two tandem aneurysms treated with flow diverters. Int J Numer Method Biomed Eng. 2014 Apr;30(4):517-24. doi: 10.1002/cnm.2614. Epub 2013 Dec 19.

Mut F, Wright S, Ascoli GA, Cebral JR. Morphometric, geographic, and territorial characterization of brain arterial trees. Int J Numer Method Biomed Eng. 2014 Jul;30(7):755-66. doi: 10.1002/cnm.2627. Epub 2014 Jan 27.

Navidbakhsh M, Rezazadeh M. 2012. An Immersed Boundary-Lattice Boltzmann Model for Simulation of Malaria-Infected Red Blood Cell in Micro-Channel. Scientia Iranica 19 (5): 1329–36.

Nowinski WL. Evolution of Human Brain Atlases in Terms of Content, Applications, Functionality, and Availability. Neuroinformatics. 2021 Jan;19(1):1-22. doi: 10.1007/s12021-020-09481-9.

Nowinski WL, Chua BC, Marchenko Y, Puspitsari F, Volkau I, Knopp MV. Three-dimensional reference and stereotactic atlas of human cerebrovasculature from 7Tesla. Neuroimage. 2011 Apr 1;55(3):986-98. doi: 10.1016/j.neuroimage.2010.12.079. Epub 2011 Jan 7.

Ospel JM, Volny O, Jayaraman M, McTaggart R, Goyal M. Optimizing fast first pass complete reperfusion in acute ischemic stroke - the BADDASS approach (BAlloon guiDe with large bore Distal Access catheter with dual aspiration with Stent-retriever as Standard approach). Expert Rev Med Devices. 2019 Nov;16(11):955-963. doi: 10.1080/17434440.2019.1684263. Epub 2019 Oct 31.

Østergaard L, Engedal TS, Aamand R, Mikkelsen R, Iversen NK, Anzabi M, Næss-Schmidt ET, Drasbek KR, Bay V, Blicher JU, Tietze A, Mikkelsen IK, Hansen B, Jespersen SN, Juul N, Sørensen JC, Rasmussen M. Capillary transit time heterogeneity and flow-metabolism coupling after traumatic brain injury. J Cereb Blood Flow Metab. 2014 Oct;34(10):1585-98. doi: 10.1038/jcbfm.2014.131. Review.

Ouared R, Chopard B. 2005. Lattice Boltzmann Simulations of Blood Flow: Non-Newtonian Rheology and Clotting Processes. Journal of Statistical Physics 121 (1): 209–21.

Paál G, Ugron A, Szikora I, Bojtár I. 2007. Flow in Simplified and Real Models of Intracranial Aneurysms. International Journal of Heat and Fluid Flow. https://doi.org/10.1016/j.ijheatfluidflow.2007.04.004.

Padmos RM, Józsa TI, El-Bouri WK, Konduri PR, Payne SJ, Hoekstra AG. Coupling one-dimensional arterial blood flow to three-dimensional tissue perfusion models for in silico trials of acute ischaemic stroke. Interface Focus. 2021 Feb 6;11(1):20190125. doi: 10.1098/rsfs.2019.0125. Epub 2020 Dec 11.

Papantchev V, Stoinova V, Aleksandrov A, Todorova-Papantcheva D, Hristov S, Petkov D, Nachev G, Ovtscharoff W. The role of Willis circle variations during unilateral selective cerebral perfusion: a study of 500 circles. Eur J Cardiothorac Surg. 2013 Oct;44(4):743-53. doi: 10.1093/ejcts/ezt103. Epub 2013 Mar 7.

Park CS, Payne SJ. Modelling the effects of cerebral microvasculature morphology on oxygen transport. Med Eng Phys. 2016 Jan;38(1):41-7. doi: 10.1016/j.medengphy.2015.09.004. Epub 2015 Oct 21.

Park CS, Hartung G, Alaraj A, Du X, Charbel FT, Linninger AA. Quantification of blood flow patterns in the cerebral arterial circulation of individual (human) subjects. Int J Numer Method Biomed Eng. 2020 Jan;36(1):e3288. doi: 10.1002/cnm.3288. Epub 2019 Dec 3.

Passat N, Ronse C, Baruthio J, Armspach JP, Maillot C. Magnetic resonance angiography: from anatomical knowledge modeling to vessel segmentation. Med Image Anal. 2006 Apr;10(2):259-74. doi: 10.1016/j.media.2005.11.002. Epub 2006 Jan 4.

Payne SJ. Cerebral autoregulation. Springer. 2016.

Payne SJ. Cerebral blood flow and metabolism. World Scientific Publishing. 2017.

Payne SJ, Lucas C. Oxygen delivery from the cerebral microvasculature to tissue is governed by a single time constant of approximately 6 seconds. Microcirculation. 2018 Feb;25(2). doi: 10.1111/micc.12428.

Payne SJ, El-Bouri WK. Modelling dynamic changes in blood flow and volume in the cerebral vasculature. Neuroimage. 2018 Aug 1;176:124-137. doi: 10.1016/j.neuroimage.2018.04.037. Epub 2018 Apr 19.

Peach TW, Ricci D, Ventikos Y. A Virtual Comparison of the eCLIPs Device and Conventional Flow-Diverters as Treatment for Cerebral Bifurcation Aneurysms. Cardiovasc Eng Technol. 2019 Sep;10(3):508-519. doi: 10.1007/s13239-019-00424-3. Epub 2019 Jul 8.

Pennings FA, Bouma GJ, Ince C. Direct observation of the human cerebral microcirculation during aneurysm surgery reveals increased arteriolar contractility. Stroke. 2004 Jun;35(6):1284-8. doi: 10.1161/01.STR.0000126039.91400.cb. Epub 2004 Apr 15.

Peyrounette M, Davit Y, Quintard M, Lorthois S. Multiscale modelling of blood flow in cerebral microcirculation: Details at capillary scale control accuracy at the level of the cortex. PLoS One. 2018 Jan 11;13(1):e0189474. doi: 10.1371/journal.pone.0189474. eCollection 2018.

Piebalgs A, Gu B, Roi D, Lobotesis K, Thom S, Xu XY. Computational Simulations of Thrombolytic Therapy in Acute Ischaemic Stroke. Sci Rep. 2018 Oct 25;8(1):15810. doi: 10.1038/s41598-018-34082-7.

Pleydell CP, David T, Smye SW, Berridge DC. A mathematical model of post-canalization thrombolysis. Phys Med Biol. 2002 Jan 21;47(2):209-24. doi: 10.1088/0031-9155/47/2/303.

Popel AS, Enden G. An analytic solution for steady flow of Quemada fluid in a circular tube. Rheol Acta. 1993;32:422-426.

Pries AR, Secomb TW. Rheology of the microcirculation. Clin Hemorheol Microcirc. 2003;29(3-4):143-8.

Pries AR, Secomb TW, Gaehtgens P, Gross JF. Blood flow in microvascular networks. Experiments and simulation. Circ Res. 1990 Oct:67(4):826-34.

Pries AR, Neuhaus D, Gaehtgens P. Blood viscosity in tube flow: dependence on diameter and hematocrit. Am J Physiol. 1992 Dec;263(6 Pt 2):H1770-8. doi: 10.1152/ajpheart.1992.263.6.H1770.

Pries AR, Secomb TW, Gaehtgens P. Biophysical aspects of blood flow in the microvasculature. Cardiovasc Res. 1996 Oct;32(4):654-67.

Pries AR, Secomb TW. Microvascular blood viscosity in vivo and the endothelial surface layer. Am J Physiol Heart Circ Physiol. 2005 Dec;289(6):H2657-64. doi: 10.1152/ajpheart.00297.2005.

Reichold J, Stampanoni M, Lena Keller A, Buck A, Jenny P, Weber B. Vascular graph model to simulate the cerebral blood flow in realistic vascular networks. J Cereb Blood Flow Metab. 2009 Aug;29(8):1429-43.

Riddle DR, Sonntag WE, Lichtenwalner RJ. Microvascular plasticity in aging. Ageing Res Rev. 2003 Apr;2(2):149-68. doi: 10.1016/s1568-1637(02)00064-8.

Rius-Pérez S, Tormos AM, Pérez S, Taléns-Visconti R. Vascular pathology: Cause or effect in Alzheimer disease? Neurologia (Engl Ed). 2018 Mar;33(2):112-120. doi: 10.1016/j.nrl.2015.07.010. Epub 2015 Sep 16.

Safaeian N, David T. A computational model of oxygen transport in the cerebrocapillary levels for normal and pathologic brain function. J Cereb Blood Flow Metab. 2013 Oct;33(10):1633-41. doi: 10.1038/jcbfm.2013.119.

Sarrami-Foroushani A, Villa-Uriol MC, Nasr Esfahany M, Coley SC, Di Marco LY, Frangi AF, Marzo A. Modeling of the acute effects of primary hypertension and hypotension on the

hemodynamics of intracranial aneurysms. Ann Biomed Eng. 2015 Jan;43(1):207-21. doi: 10.1007/s10439-014-1076-7. Epub 2014 Aug 13.

Sarrami-Foroushani A, Lassila T, Frangi AF. Virtual endovascular treatment of intracranial aneurysms: models and uncertainty. Wiley Interdiscip Rev Syst Biol Med. 2017 Jul;9(4). doi: 10.1002/wsbm.1385. Epub 2017 May 10.

Sarrami-Foroushani A, Lassila T, MacRaild M, Asquith J, Roes KCB, Byrne JV, Frangi AF. In-silico trial of intracranial flow diverters replicates and expands insights from conventional clinical trials. Nat Commun. 2021 Jun 23;12(1):3861. doi: 10.1038/s41467-021-23998-w.

Saxena A, Ng EYK, Lim ST. Imaging modalities to diagnose carotid artery stenosis: progress and prospect. Biomed Eng Online. 2019 May 28;18(1):66. doi: 10.1186/s12938-019-0685-7.

Scheffer S, Hermkens DMA, van der Weerd L, de Vries HE, Daemen MJAP. Vascular Hypothesis of Alzheimer Disease: Topical Review of Mouse Models. Arterioscler Thromb Vasc Biol. 2021 Apr;41(4):1265-1283. doi: 10.1161/ATVBAHA.120.311911. Epub 2021 Feb 25.

Schmid F, Tsai PS, Kleinfeld D, Jenny P, Weber B. Depth-dependent flow and pressure characteristics in cortical microvascular networks. PLoS Comput Biol. 2017 Feb 14;13(2):e1005392. doi: 10.1371/journal.pcbi.1005392. eCollection 2017 Feb.

Schmid F, Barrett MJP, Jenny P, Weber B. Vascular density and distribution in neocortex. Neuroimage. 2019 Aug 15;197:792-805. doi: 10.1016/j.neuroimage.2017.06.046. Epub 2017 Jun 29.

Secomb TW, Pries AR. Blood viscosity in microvessels: experiment and theory. C R Phys. 2013 Jun;14(6):470-478.

Secomb TW, Hsu R, Beamer NB, Coull BM. Theoretical simulation of oxygen transport to brain by networks of microvessels: effects of oxygen supply and demand on tissue hypoxia. Microcirculation. 2000; 7(4): 237–247.

Shapiro M, Raz E, Becske T, Nelson PK. Variable porosity of the pipeline embolization device in straight and curved vessels: a guide for optimal deployment strategy. AJNR Am J Neuroradiol. 2014 Apr;35(4):727-33. doi: 10.3174/ajnr.A3742. Epub 2013 Sep 26.

Sharan M, Popel AS. A two-phase model for flow of blood in narrow tubes with increased effective viscosity near the wall. Biorheology. 2001;38(5-6):415-28.

Sharma P, Ninomiya T, Omodaka K, Takahashi N, Miya T, Himori N, Okatani T, Nakazawa T. A lightweight deep learning model for automatic segmentation and analysis of ophthalmic images. Sci Rep. 2022 May 20;12(1):8508. doi: 10.1038/s41598-022-12486-w.

Shaw K, Boyd K, Anderle S, Hammond-Haley M, Amin D, Bonnar O, Hall CN. Gradual Not Sudden Change: Multiple Sites of Functional Transition Across the Microvascular Bed. Front Aging Neurosci. 2022 Feb 14;13:779823. doi: 10.3389/fnagi.2021.779823. eCollection 2021.

Shi Y, Lawford P, Hose R. Review of zero-D and 1-D models of blood flow in the cardiovascular system. Biomed Eng Online. 2011 Apr 26;10:33. doi: 10.1186/1475-925X-10-33.

Shipley RJ, Chapman SJ. Multiscale modelling of fluid and drug transport in vascular tumours. Bull Math Biol. 2010 Aug;72(6):1464-91. doi: 10.1007/s11538-010-9504-9. Epub 2010 Jan 23.

Shipley RJ, Sweeney PW, Chapman SJ, Roose T. A four-compartment multiscale model of fluid and drug distribution in vascular tumours. Int J Numer Method Biomed Eng. 2020 Mar;36(3):e3315. doi: 10.1002/cnm.3315. Epub 2020 Feb 25.

Shojima M, Oshima M, Takagi K, Torii R, Hayakawa M, Katada K, Morita A, Kirino T. Magnitude and role of wall shear stress on cerebral aneurysm: computational fluid dynamic study of 20 middle cerebral artery aneurysms. Stroke. 2004 Nov;35(11):2500-5. doi: 10.1161/01.STR.0000144648.89172.0f.

Skalak R. Modelling the mechanical behavior of red blood cells. Biorheology. 1973 Jun;10(2):229-38. doi: 10.3233/bir-1973-10215.

Smith NB and Webb A. Introduction to Medical Imaging. Cambridge University Press, 2011.

Smith AF, Doyeux V, Berg M, Peyrounette M, Haft-Javaherian M, Larue AE, Slater JH, Lauwers F, Blinder P, Tsai P, Kleinfeld D, Schaffer CB, Nishimura N, Davit Y, Lorthois S. Brain Capillary Networks Across Species: A few Simple Organizational Requirements Are Sufficient to Reproduce Both Structure and Function. Front Physiol. 2019 Mar 26;10:233. doi: 10.3389/fphys.2019.00233. eCollection 2019.

Steinman DA, Pereira VM. How patient specific are patient-specific computational models of cerebral aneurysms? An overview of sources of error and variability. Neurosurg Focus. 2019 Jul 1;47(1):E14. doi: 10.3171/2019.4.FOCUS19123.

Steinman DA, Vorp DA, Ethier CR. Computational modeling of arterial biomechanics: insights into pathogenesis and treatment of vascular disease. J Vasc Surg. 2003 May;37(5):1118-28. doi: 10.1067/mva.2003.122.

Su SW, Catherall M, Payne S. The influence of network structure on the transport of blood in the human cerebral microvasculature. Microcirculation. 2012;19:175–187.

Sweeney PW, Walker-Samuel S, Shipley RJ. Insights into cerebral haemodynamics and oxygenation utilising in vivo mural cell imaging and mathematical modelling. Sci Rep. 2018 Jan 22;8(1):1373. doi: 10.1038/s41598-017-19086-z.

Tahir AM, Chowdhury MEH, Khandakar A, Rahman T, Qiblawey Y, Khurshid U, Kiranyaz S, Ibtehaz N, Rahman MS, Al-Maadeed S, Mahmud S, Ezeddin M, Hameed K, Hamid T. COVID-19

infection localization and severity grading from chest X-ray images. Comput Biol Med. 2021 Dec;139:105002. doi: 10.1016/j.compbiomed.2021.105002. Epub 2021 Oct 30.

Talayero C, Romero G, Pearce G, Wong J. Numerical modelling of blood clot extraction by aspiration thrombectomy. Evaluation of aspiration catheter geometry. J Biomech. 2019 Sep 20;94:193-201. doi: 10.1016/j.jbiomech.2019.07.033. Epub 2019 Aug 7.

Tawk RG, Hasan TF, D'Souza CE, Peel JB, Freeman WD. Diagnosis and Treatment of Unruptured Intracranial Aneurysms and Aneurysmal Subarachnoid Hemorrhage. Mayo Clin Proc. 2021 Jul;96(7):1970-2000. doi: 10.1016/j.mayocp.2021.01.005. Epub 2021 May 13.

Thompson BG, Brown RD Jr, Amin-Hanjani S, Broderick JP, Cockroft KM, Connolly ES Jr, Duckwiler GR, Harris CC, Howard VJ, Johnston SC, Meyers PM, Molyneux A, Ogilvy CS, Ringer AJ, Torner J; American Heart Association Stroke Council, Council on Cardiovascular and Stroke Nursing, and Council on Epidemiology and Prevention; American Heart Association; American Stroke Association. Guidelines for the Management of Patients With Unruptured Intracranial Aneurysms: A Guideline for Healthcare Professionals From the American Heart Association/American Stroke Association. Stroke. 2015 Aug;46(8):2368-400. doi: 10.1161/STR.0000000000000070. Epub 2015 Jun 18.

Tikhvinskii D, Kuianova J, Kislitsin D, Orlov K, Gorbatykh A, Parshin D. Numerical Assessment of the Risk of Abnormal Endothelialization for Diverter Devices: Clinical Data Driven Numerical Study. J Pers Med. 2022 Apr 18;12(4):652. doi: 10.3390/jpm12040652.

Todorov MI, Paetzold JC, Schoppe O, Tetteh G, Shit S, Efremov V, Todorov-Völgyi K, Düring M, Dichgans M, Piraud M, Menze B, Ertürk A. Machine learning analysis of whole mouse brain vasculature. Nat Methods. 2020 Apr;17(4):442-449. doi: 10.1038/s41592-020-0792-1. Epub 2020 Mar 11.

Torii R, Oshima M, Kobayashi T, Takagi K, Tezduyar TE. 2008. Fluid–structure Interaction Modeling of a Patient-Specific Cerebral Aneurysm: Influence of Structural Modeling. Computational Mechanics. https://doi.org/10.1007/s00466-008-0325-8.

Toro EF, Celant M, Zhang Q, Contarino C, Agarwal N, Linninger A, Müller LO. Cerebrospinal fluid dynamics coupled to the global circulation in holistic setting: Mathematical models, numerical methods and applications. Int J Numer Method Biomed Eng. 2022 Jan;38(1):e3532. doi: 10.1002/cnm.3532. Epub 2021 Oct 19.

Tsai PS, Friedman B, Ifarraguerri AI, Thompson BD, Lev-Ram V, Schaffer CB, Xiong Q, Tsien RY, Squier JA, Kleinfeld D. All-optical histology using ultrashort laser pulses. Neuron. 2003 Jul 3;39(1):27-41. doi: 10.1016/s0896-6273(03)00370-2.

Tsai PS, Kaufhold JP, Blinder P, Friedman B, Drew PJ, Karten HJ, Lyden PD, Kleinfeld D. Correlations of neuronal and microvascular densities in murine cortex revealed by direct counting and colocalization of nuclei and vessels. Journal of Neuroscience. 2009;29:14553–14570.

Ugron Á, Farinas M, Kiss L, Paál G. 2011. Unsteady Velocity Measurements in a Realistic Intracranial Aneurysm Model. Experiments in Fluids 52 (1): 37–52.

Ugron A, Szikora I, Paál G. Measurement of flow diverter hydraulic resistance to model flow modification in and around intracranial aneurysms. Interv Med Appl Sci. 2014 Jun;6(2):61-8. doi: 10.1556/IMAS.6.2014.2.2. Epub 2014 Jun 4.

Ungvari Z, Kaley G, de Cabo R, Sonntag WE, Csiszar A. Mechanisms of vascular aging: new perspectives. J Gerontol A Biol Sci Med Sci. 2010 Oct;65(10):1028-41. doi: 10.1093/gerona/glq113. Epub 2010 Jun 24.

Uryga A, Kasprowicz M, Calviello L, Diehl RR, Kaczmarska K, Czosnyka M. Assessment of cerebral hemodynamic parameters using pulsatile versus non-pulsatile cerebral blood outflow models. J Clin Monit Comput. 2019 Feb;33(1):85-94. doi: 10.1007/s10877-018-0136-1. Epub 2018 Apr 4.

Vaitkevicius PV, Fleg JL, Engel JH, O'Connor FC, Wright JG, Lakatta LE, Yin FC, Lakatta EG. Effects of age and aerobic capacity on arterial stiffness in healthy adults. Circulation. 1993 Oct;88(4 Pt 1):1456-62. Doi: 10.1161/01.cir.88.4.1456.

van Beek AH, Claassen JA, Rikkert MG, Jansen RW. Cerebral autoregulation: an overview of current concepts and methodology with special focus on the elderly. J Cereb Blood Flow Metab. 2008 Jun;28(6):1071-85. doi: 10.1038/jcbfm.2008.13. Epub 2008 Mar 19.

Valencia A, Burdiles P, Ignat M, Mura J, Bravo E, Rivera R, Sordo J. Fluid structural analysis of human cerebral aneurysm using their own wall mechanical properties. Comput Math Methods Med. 2013;2013:293128. doi: 10.1155/2013/293128. Epub 2013 Sep 18.

van Rooij BJM, Závodszky G, Hoekstra AG, Ku DN. Haemodynamic flow conditions at the initiation of high-shear platelet aggregation: a combined in vitro and cellular in silico study. Interface Focus. 2021 Feb 6;11(1):20190126. doi: 10.1098/rsfs.2019.0126. Epub 2020 Dec 11.

Vardakis JC, Chou D, Tully BJ, Hung CC, Lee TH, Tsui PH, Ventikos Y. Investigating cerebral oedema using poroelasticity. Med Eng Phys. 2016 Jan;38(1):48-57. doi: 10.1016/j.medengphy.2015.09.006. Epub 2015 Dec 31.

Vardakis JC, Bonfanti M, Franzetti G, Guo L, Lassila T, Mitolo M, Hoz de Vila M, Greenwood JP, Maritati G, Chou D, Taylor ZA, Venneri A, Homer-Vanniasinkam S, Balabani S, Frangi AF, Ventikos Y, Diaz-Zuccarini V. Highly integrated workflows for exploring cardiovascular conditions: Exemplars of precision medicine in Alzheimer's disease and aortic dissection. Morphologie. 2019 Dec;103(343):148-160. doi: 10.1016/j.morpho.2019.10.045. Epub 2019 Nov 27.

Vardakis JC, Chou D, Guo L, Ventikos Y. Exploring neurodegenerative disorders using a novel integrated model of cerebral transport: Initial results. Proc Inst Mech Eng H. 2020 Nov;234(11):1223-1234. doi: 10.1177/0954411920964630. Epub 2020 Oct 20.

Viceconti M, Hunter P. The Virtual Physiological Human: Ten Years After. Annu Rev Biomed Eng. 2016 Jul 11;18:103-23. doi: 10.1146/annurev-bioeng-110915-114742.

Villa-Uriol MC, Berti G, Hose DR, Marzo A, Chiarini A, Penrose J, Pozo J, Schmidt JG, Singh P, Lycett R, Larrabide I, Frangi AF. @neurIST complex information processing toolchain for the integrated management of cerebral aneurysms. Interface Focus. 2011 Jun 6;1(3):308-19. doi: 10.1098/rsfs.2010.0033. Epub 2011 Apr 6.

Viviani R. A Digital Atlas of Middle to Large Brain Vessels and Their Relation to Cortical and Subcortical Structures. Front Neuroanat. 2016 Feb 17;10:12. doi: 10.3389/fnana.2016.00012. eCollection 2016.

Wang R, Li C, Wang J, Wei X, Li Y, Zhu Y, Zhang S. Threshold segmentation algorithm for automatic extraction of cerebral vessels from brain magnetic resonance angiography images. J Neurosci Methods. 2015 Feb 15;241:30-6. doi: 10.1016/j.jneumeth.2014.12.003. Epub 2014 Dec 11.

Wardlaw JM, Murray V, Berge E, del Zoppo G, Sandercock P, Lindley RL, Cohen G. Recombinant tissue plasminogen activator for acute ischaemic stroke: an updated systematic review and meta-analysis. Lancet. 2012 Jun 23;379(9834):2364-72. doi: 10.1016/S0140-6736(12)60738-7. Review.

Wardlaw JM, Smith EE, Biessels GJ, Cordonnier C, Fazekas F, Frayne R, Lindley RI, O'Brien JT, Barkhof F, Benavente OR, Black SE, Brayne C, Breteler M, Chabriat H, Decarli C, de Leeuw FE,

Doubal F, Duering M, Fox NC, Greenberg S, Hachinski V, Kilimann I, Mok V, Oostenbrugge Rv, Pantoni L, Speck O, Stephan BC, Teipel S, Viswanathan A, Werring D, Chen C, Smith C, van Buchem M, Norrving B, Gorelick PB, Dichgans M; STandards for ReportIng Vascular changes on nEuroimaging (STRIVE v1). Neuroimaging standards for research into small vessel disease and its contribution to ageing and neurodegeneration. Lancet Neurol. 2013 Aug;12(8):822-38. doi: 10.1016/S1474-4422(13)70124-8.

Wardlaw JM, Brazzelli M, Chappell FM, Miranda H, Shuler K, Sandercock PA, Dennis MS. ABCD2 score and secondary stroke prevention: meta-analysis and effect per 1,000 patients triaged. Neurology. 2015 Jul 28;85(4):373-80. doi: 10.1212/WNL.0000000000001780. Epub 2015 Jul 1.

Weafer FM, Duffy S, Machado I, Gunning G, Mordasini P, Roche E, McHugh PE, Gilvarry M. Characterization of strut indentation during mechanical thrombectomy in acute ischemic stroke clot analogs. J Neurointerv Surg. 2019 Sep;11(9):891-897. doi: 10.1136/neurintsurg-2018-014601. Epub 2019 Jan 19.

Weber B, Keller AL, Reichold J, Logothetis NK. The microvascular system of the striate and extrastriate visual cortex of the macaque. Cerebral Cortex. 2008;18:2318–2330.

Weir B, Disney L, Karrison T. Sizes of ruptured and unruptured aneurysms in relation to their sites and the ages of patients. J Neurosurg. 2002 Jan;96(1):64-70. doi: 10.3171/jns.2002.96.1.0064.

Womersley, JR. Method for the calculation of velocity, rate of flow and viscous drag in arteries when the pressure gradient is known. J Physiol. 1955 Mar 28;127(3):553-63.

Wootton DM, Popel AS, Alevriadou BR. An experimental and theoretical study on the dissolution of mural fibrin clots by tissue-type plasminogen activator. Biotechnol Bioeng. 2002 Feb 15;77(4):405-19.

Wright SN, Kochunov P, Mut F, Bergamino M, Brown KM, Mazziotta JC, Toga AW, Cebral JR, Ascoli GA. Digital reconstruction and morphometric analysis of human brain arterial vasculature from magnetic resonance angiography. Neuroimage. 2013 Nov 15;82:170-81. doi: 10.1016/j.neuroimage.2013.05.089. Epub 2013 May 28.

Xie L, Kang H, Xu Q, Chen MJ, Liao Y, Thiyagarajan M, O'Donnell J, Christensen DJ, Nicholson C, Iliff JJ, Takano T, Deane R, Nedergaard M. Sleep drives metabolite clearance from the adult brain. Science. 2013 Oct 18;342(6156):373-7. doi: 10.1126/science.1241224.

Xu X, Wang B, Ren C, Hu J, Greenberg DA, Chen T, Xie L, Jin K. Age-related Impairment of Vascular Structure and Functions. Aging Dis. 2017 Oct 1;8(5):590-610. doi: 10.14336/AD.2017.0430. eCollection 2017 Oct.

Xue S, Gong H, Jiang T, Luo W, Meng Y, Liu Q, Chen S, Li A. Indian-ink perfusion based method for reconstructing continuous vascular networks in whole mouse brain. PLoS One. 2014 Jan 30;9(1):e88067. doi: 10.1371/journal.pone.0088067. eCollection 2014.

Xue Y, El-Bouri WK, Józsa TI, Payne SJ. Modelling the effects of cerebral microthrombi on tissue oxygenation and cell death. J Biomech. 2021 Oct 11;127:110705. doi: 10.1016/j.jbiomech.2021.110705. Epub 2021 Aug 23.

Xue Y, Georgakopoulou T, van der Wijk AE, Józsa TI, van Bavel E, Payne SJ. Quantification of hypoxic regions distant from occlusions in cerebral penetrating arteriole trees. PLoS Comput Biol. 2022 Aug 5;18(8):e1010166. doi: 10.1371/journal.pcbi.1010166. eCollection 2022 Aug.

Yu R, Deng M, Yap PT, Wei Z, Wang L, Shen D. Learning-Based 3T Brain MRI Segmentation with Guidance from 7T MRI Labeling. Mach Learn Med Imaging. 2016 Oct;10019:213-220. doi: 10.1007/978-3-319-47157-0_26. Epub 2016 Oct 1.

Závodszky G, Paál G. 2013. Validation of a Lattice Boltzmann Method Implementation for a 3D Transient Fluid Flow in an Intracranial Aneurysm Geometry. International Journal of Heat and Fluid Flow. https://doi.org/10.1016/j.ijheatfluidflow.2013.06.008.

Závodszky G, van Rooij B, Azizi V, Hoekstra A. Cellular Level In-silico Modeling of Blood Rheology with An Improved Material Model for Red Blood Cells. Front Physiol. 2017 Aug 2;8:563. doi: 10.3389/fphys.2017.00563. eCollection 2017.

Zagzoule M, Marc-Vergnes JP. A global mathematical model of the cerebral circulation in man. J Biomech. 1986;19(12):1015-22.

Zhao Y, Liu Y, Wu X, Harding SP, Zheng Y. Retinal vessel segmentation: an efficient graph cut approach with retinex and local phase. PLoS One. 2015 Apr 1;10(4):e0122332. doi: 10.1371/journal.pone.0122332. eCollection 2015.

Zhao Y, Zheng Y, Liu Y, Zhao Y, Luo L, Yang S, Na T, Wang Y, Liu J. Automatic 2-D/3-D Vessel Enhancement in Multiple Modality Images Using a Weighted Symmetry Filter. IEEE Trans Med Imaging. 2018 Feb;37(2):438-450. doi: 10.1109/TMI.2017.2756073. Epub 2017 Sep 25.

Zhang Y, Furusawa T, Sia SF, Umezu M, Qian Y. Proposition of an outflow boundary approach for carotid artery stenosis CFD simulation. Comput Methods Biomech Biomed Engin. 2013;16(5):488-94. doi: 10.1080/10255842.2011.625358. Epub 2012 Jan 30.

Zhou Q, Schirrmann K, Doman E, Chen Q, Singh N, Selvaganapathy PR, Bernabeu MO, Jensen OE, Juel A, Chernyavsky, Kruger T. Red blood cell dynamics in extravascular biological tissues modelled as canonical disordered porous media. 2022. Interface Focus.122022003720220037 http://doi.org/10.1098/rsfs.2022.0037